Received: 12 April 2023 | Revised: 11 July 2023 | Accepted: 19 July 2023

DOI: 10.1111/cbdd.14314

RESEARCH ARTICLE

WILEY

Cytotoxic activity of quinolinequinones in cancer: In vitro studies, molecular docking, and ADME/PK profiling

Ayse Tarbin Jannuzzi[1] | **Ayse Mine Yilmaz Goler**[2] | **Deepak Shilkar**[3] | **Subodh Mondal**[4] | **Vinay N. Basavanakatti**[5] | **Hatice Yıldırım**[6] | **Mahmut Yıldız**[7] | **Hülya Çelik Onar**[6] | **Nilüfer Bayrak**[8] | **Venkatesan Jayaprakash**[3] | **Amaç Fatih TuYuN**[8]

[1]Faculty of Pharmacy, Department of Pharmaceutical Toxicology, İstanbul University, Istanbul, Turkey

[2]Department of Biochemistry, School of Medicine/Genetic and Metabolic Diseases Research and Investigation Center, Marmara University, Istanbul, Turkey

[3]Department of Pharmaceutical Sciences & Technology, Birla Institute of Technology, Mesra, Ranchi, Jharkhand, India

[4]Bioanalysis, Eurofins Advinus BioPharma Services India Pvt Ltd., Bengaluru, Karnataka, India

[5]Adgyl Lifesciences Private Limited, Bengaluru, Karnataka, India

[6]Department of Chemistry, Engineering Faculty, Istanbul University-Cerrahpasa, Istanbul, Turkey

[7]Department of Chemistry, Gebze Technical University, Kocaeli, Turkey

[8]Department of Chemistry, Faculty of Science, Istanbul University, Istanbul, Turkey

Correspondence
Amaç Fatih TuYuN, Department of Chemistry, Faculty of Science, Istanbul University, Fatih, 34126, Istanbul, Turkey.
Email: aftuyun@gmail.com, aftuyun@istanbul.edu.tr

Abstract

Lead molecules containing 1,4-quinone moiety are intriguing novel compounds that can be utilized to treat cancer owing to their antiproliferative activities. Nine previously reported quinolinequinones (**AQQ1-9**) were studied to better understand their inhibitory profile to produce potent and possibly safe lead molecules. The National Cancer Institute (NCI) of Bethesda chose all quinolinequinones (**AQQ1-9**) based on the NCI Developmental Therapeutics Program and tested them against a panel of 60 cancer cell lines. At a single dose and five further doses, **AQQ7** significantly inhibited the proliferation of all leukemia cell lines and some breast cancer cell lines. We investigated the in vitro cytotoxic activities of the most promising compounds, **AQQ2** and **AQQ7**, in MCF7 and T-47D breast cancer cells, DU-145 prostate cancer cells, HCT-116 and COLO 205 colon cancer cell lines, and HaCaT human keratinocytes using the MTT assay. **AQQ7** showed particularly high cytotoxicity against MCF7 cells. Further analysis showed that **AQQ7** exhibits anticancer activity through the induction of apoptosis without causing cell cycle arrest or oxidative stress. Molecular docking simulations for **AQQ2** and **AQQ7** were conducted against the COX, PTEN, and EGFR proteins, which are commonly overexpressed in breast, cervical, and prostate cancers. The in vitro ADME and in vivo PK profiling of these compounds have also been reported.

KEYWORDS

ADME, anticancer activity, breast cancer, cytotoxicity, leukemia, molecular docking

1 | INTRODUCTION

Cancer is a process of cellular transformation in which normal cells evolve into malignant cells owing to genetic changes (Markopoulos et al., 2017; van Oijen & Slootweg, 2000). Chemicals, viruses, radiation, nutritional restriction, and radiation can cause gene changes in addition to those that affect signaling molecules (Brady et al., 2022; Dasari et al., 2021). In recent years, the main objective of clinical oncologists has been to develop novel

therapies that enable the efficient eradication of cancer cells. It is well recognized that immune surveillance, DNA damage, and cellular stress are some of the conditions that cause this cell death process to be mediated by several signaling channels and that some pathways interact with other signaling systems to affect cell death. The basic building blocks for developing efficient agents include studies on drug discovery addressing stability, toxicity profiles in non-malignant tissues, bioavailability, drug interactions, tumor penetration, off-target effects, and a thorough understanding of tumor biology (Carneiro & El-Deiry, 2020).

Depending on various factors, such as the type and stage of cancer, the general health profile and preferences of the patient, primary treatment such as surgery, adjuvant treatment such as chemotherapy and radiotherapy, or palliative treatment methods can be used for the physical, psychological, mental, and social needs of the patient in cancer treatment. The serious side effects of the drugs used and the rising resistance to classic chemotherapeutic agents and/or novel targeted therapies continue to be major concerns in cancer therapy, notwithstanding recent successes in cancer treatment (Alfarouk et al., 2015; Holohan et al., 2013; Housman et al., 2014). The drawbacks of being non-specific and having relatively high toxicity arise from the use of classical chemotherapeutic anticancer agents for cancer cell death that directly damage DNA (Cheung-Ong et al., 2013). Therefore, it has gained great importance in recent years to develop new, more effective, and selective drugs that precisely target or block the changes that cause cancer growth and proliferation. Natural products are crucial for the discovery and development of novel therapeutics for cancer treatment; however, with the advancement of synthetic pharmaceutical chemistry, new molecules with enormous chemical diversity and promising biological activities have also emerged as top targets of the scientific community (Bayrak et al., 2020; Bayrak et al., 2019; Ciftci et al., 2019; Kimura, 2005; Majolo et al., 2019).

The most significant medical concern currently faced by women is breast cancer. Breast cancer, which has long been known to be the major cause of cancer-related deaths in women, has once again demonstrated how dangerous it is after overtaking lung cancer in the World Health Organization's 2021 data to become the cancer type most often diagnosed worldwide. One in four cancer cases in women and one in six cancer-related deaths are due to breast cancer. The estimated age-standardized incidence rate (World) of breast cancer in 2020 worldwide for both sexes is 47.8 (World Cancer Day, 2021). Breast cancer prevention is challenging because the reasons for this are not fully understood. Numerous risk factors, including nulliparity, late age at first pregnancy, and little to no nursing, are associated with the historical growth of human civilization (Veronesi & Boyle, 2017). Therefore, great efforts are needed to discover new lead molecules to treat breast cancer.

Previously, we focused on discovering novel anticancer prototypes for the treatment of breast cancer and discovered a new family of chemicals called substituted 1,4-quinones as members of plastoquinone analogs (Jannuzzi et al., 2021, 2022; Yilmaz Goler et al., 2022). This study aimed to further this inquiry using a structure-based drug design strategy to identify new inhibitors for breast cancer treatment. A collection of compounds with quinolinequinone scaffolds that have been variously substituted with different moieties was first considered. The nature and position of the substituents on the arylamine moiety were also manipulated. Nine target quinolinequinones were synthesized and submitted to the National Cancer Institute (NCI) of Bethesda within the Developmental Therapeutics Program (DTP) and screened against the NCI panel of 60 cancer cell lines (Ricci & Zong, 2006) at a single dose (10 μM) for nine different cancer types, including leukemia, lung, colon, CNS, melanoma, ovarian, renal, prostate, and breast cancer cell lines (Boyd & Paull, 1995), using the protocol of the Drug Evaluation Branch, NCI (Razaghi et al., 2018). The DTP division of the NCI selected four quinolinequinones (**AQQ2**, **AQQ6**, **AQQ7**, and **AQQ9**) for a complete panel five-dose in vitro assay to ascertain their GI_{50} in 60 cell lines following a single-dose assessment. Encouraged by the NCI results, two quinolinequinones (**AQQ2** and **AQQ7**) were tested for cytotoxicity against MCF7 and T-47D breast cancer cells, DU145 prostate cancer cells, HCT-116 cells, and COLO 205 colon cancer cell lines. HaCaT human keratinocytes were used as a non-cancerous cell line to evaluate cancer selectivity. Furthermore, we investigated the effects of quinolinequinone (**AQQ7**) on cell proliferation, apoptosis, and reactive oxygen species (ROS) production in MCF7 breast cancer cells. To further investigate the host–guest interactions of potent quinolinequinones, thorough in silico docking simulations were conducted.

2 | METHODS AND MATERIALS

2.1 | Biological evaluation

2.1.1 | In vitro single-dose anticancer screening by NCI

The obtained quinolinequinones were submitted to the National Cancer Institute (NCI), Bethesda, USA, and according to the standard protocol of NCI, all compounds were evaluated for their antiproliferative activity in a single-dose assay (10 μM concentration in DMSO) on a

panel of 60 cancer cell lines derived from leukemia, non-small cell lung, colon, CNS, melanoma, ovarian, renal, prostate, and breast as per protocol. The test compounds were added to microtiter culture plates and incubated for 48 h at 37°C. Sulforhodamine B (SRB), a protein-binding dye, was used for end-point determination. The percentage of growth of the treated cells was compared to that of the untreated control cells, and the results for each tested compound are reported. Data from one-dose experiments pertained to growth percentage at 10 μM (Boyd & Paull, 1995; Grever et al., 1992; Monks et al., 1991).

2.1.2 | In vitro five-dose anticancer screening by NCI

Serial 5×10-fold dilutions of an initial DMSO stock solution were performed before incubation at each concentration. The most promising quinolinequinones (**AQQ2**, **AQQ6**, **AQQ7**, and **AQQ9**) were then elevated by DTP-NCI at a higher testing level to determine three dose–response parameters (GI_{50}, TGI, and LC_{50}) for each cell line after establishing a dose–response curve for five different concentrations (0.01, 0.1, 1, 10, and 100 μM) of **AQQ2**, **AQQ6**, **AQQ7**, and **AQQ9**. The detailed procedure for the latter assay has been previously described (Boyd & Paull, 1995; Grever et al., 1992; Monks et al., 1991).

2.1.3 | Cell culture

MCF7 cells were grown in DMEM:F12 (Gibco). T-47D, DU-145, HCT-116, and HaCaT cells were grown in GlutaMAX DMEM (Gibco). COLO 205 cells were grown in RPMI medium (Gibco). All media were supplemented with 10% fetal bovine serum (FBS) and 1% penicillin–streptomycin in a humidified incubator at 37°C and 5% CO_2.

2.1.4 | Cytotoxicity assay

Cell viability was estimated using 3-(4,5-dimethylthiazol-2-yl)-2,5-diphenyl tetrazolium bromide (MTT) dye. Briefly, the cells were seeded in 96-well plates (1×10^4 cells/well) and cultured overnight. Different concentrations of the compounds (1–100 μM) were added to the wells, and the cells were cultured for 24 h. MTT dye (5 mg/mL) was then added, and the cells were incubated for 3 h. The supernatants were discarded, and the precipitated dye was dissolved in DMSO. The absorbance was measured at 590 nm using a microplate reader (Epoc Biotek). The half-maximal inhibitory concentrations (IC_{50}) were estimated using GraphPad software (version 7.0).

2.1.5 | Apoptotic and necrotic cell analysis

MCF7 cells were seeded in 6-well plates (3×10^5 cells/well) and incubated overnight. For the assay, the cells were treated with 0.5, 1, and 2.5 μM **AQQ7** and 2.5 μM adriamycin (ADRI), and the control for 24 h. The cells were collected and stained with the Annexin V-FITC Apoptosis Detection Kit (Millipore) following the manufacturer's protocols. Briefly, cells were resuspended in Annexin V binding buffer and stained with Annexin V-FITC and propidium iodide (PI) for 15 min at room temperature in the dark. Subsequently, BD FACS Calibur flow cytometry was performed, and results were calculated using the Cell Quest Pro 6.0 program (BD Bioscience).

2.1.6 | Cell cycle analysis

MCF7 cells were seeded in 6-well plates (3×10^5 cells/well) and incubated for 24 h for adhesion. **AQQ7** was added to the wells at concentrations of 0.5, 1, and 2.5 μM concentration and incubated for 24 h. Cells were washed twice with cold PBS and fixed with 70% ethanol for 2 h at 4°C. The cells were resuspended in an assay buffer containing 20 μg/mL PI and 50 μg/mL RNase. Cell cycle stages were analyzed by flow cytometer, BD FACS Calibur (BD Bioscience), and calculated using Cell Quest Pro 6.0 program (BD Bioscience).

2.1.7 | Oxidative stress assay

General reactive oxygen species (ROS) measurements were performed using 2, 7-dichlorodihydrofluorescein diacetate (H_2DCFDA) staining. Cells were seeded in 6-well plates (3×10^5 cells/well), and **AQQ7** was applied at 0.5, 1, and 2.5 μM concentrations for 24 h. As a positive control, H_2O_2 was added to the wells at 100 μM for 30 min of incubation. At the end of the incubation period, the cells were washed twice with PBS, incubated with 10 μM H_2DCFDA for 30 min in the dark, and immediately analyzed by flow cytometry (BD FACS Calibur) and calculated using Cell Quest Pro 6.0 program (BD Bioscience).

2.2 | In silico studies

2.2.1 | ADME

We used ADMETlab 2.0 to evaluate the ADMET properties, physicochemical properties, and medicinal chemistry friendliness of the chemical compounds under investigation. ADMETlab 2.0 is a web-based platform that utilizes

predictive models and algorithms to comprehensively evaluate the ADMET properties of chemical compounds. We inputted the SMILES notation of the compound into the ADMETlab 2.0 interface and used the available modules to obtain information on permeability, bioavailability, plasma protein binding, distribution volume, and fraction unbound. We also analyzed the toxicity profile of the compound using the toxicity prediction modules of ADMETlab 2.0. The resulting data were analyzed and interpreted to gain insights into the compound's ADMET properties, which were then compared with in vitro data.

2.2.2 | Molecular docking

The protein structures used in this study were retrieved from the Protein Data Bank (PDB) using the following codes: Epidermal Growth Factor Receptor (EGFR), 1M17 (Stamos et al., 2002); cyclooxygenase 2 (COX-2) 6BL4 (Xu et al., 2019); and phosphatase and tensin homolog (PTEN), 1D5R (Mctigue et al., 1993). Prior to docking, protein structures were prepared using the UCSF Chimera DockPrep module (Pettersen et al., 2004) with default settings (adding missing atoms, removing solvent molecules, adding hydrogen, and optimizing protein conformation to minimize steric clashes). The docking simulations were performed using AMDock wrapper (Valdes-Tresanco et al., 2020) for AutoDock 4 with the following parameters: random initial coordinates, random initial orientation and dihedrals, 3 torsional degrees of freedom, a cluster tolerance of 2.0 Å, an external grid energy of 1000.0 kcal/mol, a maximum initial energy of 0.0 kcal/mol and a maximum of 10,000 retries, a population size of 150 individuals, a maximum of 2,500,000 energy evaluations, and a maximum of 27,000 generations. The GA algorithm was used with a crossover rate of 0.8, mutation rate of 0.02, and a window size of 10. The Solis and Wets local search was performed with a maximum of 300 iterations, a maximum of four consecutive successes or failures before changing rho, a sample size of the local search space to a sample of 1.0 Å, and a lower bound on rho of 0.01 Å. Pseudo-Solis and Wets parameters were set for this algorithm. Docking simulations were run for 100 hybrid GA-LS runs, and ranked cluster analysis was performed to analyze the results.

Molecular docking data analysis was performed using two software packages: the Protein-Ligand Interaction Profiler (PLIP) (Adasme et al., 2021) and LigPlot+ (Laskowski & Swindells, 2011). PLIP v2.2.2 was utilized to identify the intermolecular interactions between the protein and ligand. LigPlot+ was used to generate 2D representations of protein–ligand interactions.

2.3 | In vivo pharmacokinetic study

2.3.1 | In vitro metabolic stability study

The liver microsomes of mice (Cat. No. M1000, Lot. No. 1710069), rats (Sprague–Dawley male, Cat. No. R1000, Lot. No. 1610290), dogs (beagle, male, Cat. No. D1000, Lot. no. 1310086), and humans (Cat. No. H0610, Lot. No. 1610016) from Xeno Tech LLC, Kansas, USA, were used to test the metabolic stability of **AQQ2**. A final protein (liver microsomal) concentration of 0.5 mg/mL and a final test substance (**AQQ2**) concentration of 0.5 μM were used for the study. To the respective microsomes at a volume of 12.5 μL in the well, 2.5 μL of **AQQ2** (100 μM in acetonitrile: dimethyl sulfoxide, 96:4) in the presence and absence of NADPH (50 μL, 10 mM) was added and the final volume made up to 500 μL with sodium phosphate buffer (50 mM, pH 7.4). A sample without NADPH served as a control. Sampling (50 μL) was performed at the following time points:0, 5, 10, 15, and 30 min for the sample, and at 0 and 30 min for the control. Acetonitrile (150 μL) was used as the quenching solvent; an internal standard (Rolipram) was added and vortexed; and an aliquot from the supernatant was analyzed using LC–MS/MS. All experiments were performed in duplicates (Figure S1).

2.3.2 | In vivo bioavailability study of **AQQ2** in male Sprague–Dawley rats

Sprague–Dawley rats (HyLasco Biotechnology (India) Pvt. Ltd., a subsidiary of Charles River from the US) of 8–12 weeks of age, weighing between 220 and 320 g, were used in this study. Animals were housed in polysulfonate cages in a typical research laboratory environment at 25 ± 3°C and 50%–70% relative humidity with approximately 12 h light and dark cycles maintained with an enrichment device. During the study, the animals had access to a rat maintenance diet (Altromin Spezialfutter GmbH, Germany) and purified water (UV-treated, charcoal-filtered). Animal experiments were conducted in accordance with the guidelines of the Committee for the Purpose of Control and Supervision of Experiments on Animals (CPCSEA), Ministry of Social Justice and Environment, Government of India, and approved by the Institutional Animal Ethics Committee. All rats were cannulated with the jugular vein, fasted overnight before dosing (except IV dose), and had access to food and water for ~4 h post-dosing. **AQQ2** in NMP (10%) + PBS (pH 7.4) qs was administered intravenously at a dose of 1 mg/kg bw (10 mL/kg). **AQQ2** in NMP (10%) + Cremophor EL (5%) + PEG400 (30%) + PG (20%) + PBS (pH 7.4) qs was administered PO at a dose of 5 mg/kg bw (10 mL/kg). The animal weight

on the day of dosing was used to calculate the required volume of the formulation and administered to the rats. After dosing, blood samples (~0.250 mL) were collected from the jugular vein at the following time points:0.083 (IV only), 0.25, 0.5, 1, 2, 4, 6, 8, and 24 h using a serial sampling design (equal volumes of heparinized saline were replaced after each sample collection). The samples were collected in pre-labeled microcentrifuge tubes containing K2EDTA (20 µL of 200 mM solution per mL of blood) as an anticoagulant. The blood samples were stored at −60°C until bioanalysis using the fit-for-purpose LC–MS/MS method. Pharmacokinetic parameters were calculated using the non-compartmental analysis (NCA) tool of the validated Phoenix® WinNonlin® 8.3.

2.3.3 | Bioanalytical method (LC/MS/MS) for AQQ2

Chemicals and reagents

MS-grade (≥99.0% pure) ammonium formate and formic acid were obtained from Sigma Aldrich. HPLC-grade acetonitrile (ACN) and dimethyl sulfoxide solvents were purchased from Merck, Germany. Milli-Q® water used for the preparation of the mobile phase, rinsing solvent, and seal washes was obtained from the in-house (Eurofins Advinus Limited) Milli-Q® system. The internal standard QDM4 ($C_{17}H_{13}ClN_2O_3$, 328.74, purity ≥97%) used in this study was procured from Sigma-Aldrich. A SCIEX API 4000™ LC/MS/MS triple quadrupole mass spectrometer system equipped with a negative electrospray ionization (ESI) source and Shimadzu prominence HPLC comprising binary pumps, a column oven, and an SIL-HTC autosampler was used in this study. Data acquisition, integration, and quantification were performed using Analyst® 1.6.3.

Chromatographic and mass spectrometric conditions

Liquid chromatographic separations of **AQQ2** and the internal standard, QDM4, were achieved on a reverse-phase Synergi Fusion RP 50 × 4.6 mm, 5 µm column operating at 40°C. The gradient mobile phase was used starting with an initial 90:10, 3 min:10:90, 6 min:10:90, and 6–10 min:90:10 for up to 8 min. Additionally, 5 mM ammonium formate with 0.1% formic acid (Mobile phase A) and 0.1% formic acid in Acetonitrile (Mobile phase B) was delivered at a flow rate of 0.6 mL/min without a splitter. The mass spectrometer was operated in negative electrospray ionization mode with unit mass resolution in a quadrupole analyzer with a dwell time of 200 ms, and the analytes were detected using multiple reaction monitoring (MRM). The compound parameters **AQQ2** and QDM4 (internal standard) were optimized along with the MRM transition (m/z) to achieve sensitivity. The source parameters were optimized to a curtain gas N_2 flow of 25 psi (CUR), nebulizer N_2 gas at 40 psi (gas 1), ion spray voltage of +5500 V (IS), auxiliary N_2 gas of 60 psi (gas 2) with a turbo spray temperature of 450°C (TEMP), and collision-activated dissociation gas (CAD) of 10 psi. The MRM transition (m/z) selected for the analyte **AQQ2** was 359.10 and 300.30, and QDM4 (internal standard) was 370.10 and 148.10. A system suitability test was performed prior to sample analysis. The system suitability test comprised six replicate injections of the extracted ULOQ and an extracted blank and LLOQ sample from rat plasma (Figures S2 and S3). The percentage coefficient of variation (CV (%)) for the peak area ratio (analyte to internal standard) of six replicate injections was ≤5%, meeting the acceptance criteria. The retention time was within ±0.5 min variation in each analytical run.

Sample preparation: **AQQ2** and QDM4 (internal standard) were extracted from rat plasma samples using the protein precipitation (crashing) method. To 50 µL of CC/QC/study samples, 200 µL of Internal Standard Working Solution in acetonitrile was added to all the tubes except for the Standard Blank sample and vortexed to mix. Vortex (Vibramax 100, Heidolph Instruments) was applied for approximately 10 min. The samples were centrifuged (Eppendorf 5810R) for 10 min at 10,000 rpm at a set temperature of 4°C. A sufficient volume of supernatant was aliquoted into autosampler vials for LC–MS/MS analysis (SCIEX API 4000).

Preparation of calibration standards and quality control samples

Stock solutions of **AQQ2** and QDM4 (internal standards) were prepared in dimethyl sulfoxide (DMSO) and acetonitrile at a concentration of 1 mg/mL. The stock solution of **AQQ2** was further diluted using DMSO to prepare calibration standard solutions in the concentration range of 20–25,000 ng/mL (Figure S4). Acetonitrile was used as an internal standard to prepare a working solution with a concentration of 500 ng/mL. These solutions were then spiked into interference-free rat blank plasma to obtain calibration standards in the pharmacologically relevant range (1–1250 ng/mL). Similarly, the quality control (QC) samples were prepared using independent stock solutions of analytes to obtain concentrations of 3.00, 500, and 1000 ng/mL in rat plasma, representing low, medium, and high concentration QC samples, respectively. Stock solutions, diluted standard solutions, quality control solutions, and internal standard solutions were stored at 2–8°C. Spiked plasma samples (calibration standards and quality controls) were freshly prepared prior to sample analysis.

3 | RESULTS AND DISCUSSION

3.1 | Chemistry

1,4-Quinone moiety has occupied a unique role in the design and discovery of biologically active molecules with remarkable medicinal activity (Borba-Santos et al., 2022; Dahlem Junior et al., 2022; Dos Santos et al., 2022; Mahalapbutr et al., 2022; Wellington, 2015). 1,4-Quinone moiety is an attractive building block for pharmaceutical research because it is present in the structures of versatile potent drugs (Basset et al., 2017; Gupta et al., 2021; Okeke et al., 2005). It is well known that inserting sulfanyl, alkoxy, and/or amino group(s) into the quinone moiety improves its physical, chemical, and biological properties (Ibacache et al., 2016; Ibis et al., 2011; Kadela et al., 2016; Nagar & Dhar, 2022). Reactions between 1,4-quinones and amines that address biologically important lead molecules have been extensively reported (Lima et al., 2021; Lopez-Lira et al., 2021; Pauli et al., 2023; Uysal et al., 2021; Varricchio et al., 2020; Yildirim et al., 2022). In line with these studies, we investigated halogenated (brominated and chlorinated) and non-halogenated plastoquinone (PQ) analogs to understand their antiproliferative profiles against breast cancer cell lines (Jannuzzi et al., 2021, 2022; Yilmaz Goler et al., 2022). Earlier studies motivated us to use the quinolinequinone moiety as the main framework for our new molecules. Encouraged by previous results with PQ analogs, especially in breast cancer cell lines (Jannuzzi et al., 2021, 2022; Yildirim et al., 2022), we introduced aryl amines containing different ester groups at different positions into the quinolinequinone moiety. The process of converting commercially available hydroxyquinoline (**HQ**) into quinolinequinone (**QQ**) in one step using sodium chlorate in concentrated HCl solution was the first step in the synthesis of aminated QQs (**AQQ1-9**), as described in Scheme 1 (Shaikh et al., 1986). The aminated QQs (**AQQ1-9**) were then regioselectively generated after treatment with the appropriate aryl amines with an ester group in the presence of the catalyst $CeCl_3.7H_2O$, according to previously described methods (Y. S. Kim et al., 2003). All aminated QQs (**AQQ1-9**) were previously reported by our group (Yildirim et al., 2022).

3.2 | Biological activities

3.2.1 | Preliminary in vitro single dose anticancer screening

In medicinal chemistry, the biological potency of a lead molecule changes with modifications to the pharmacophoric moieties. The versatility of quinone chemistry in drug development is extensive (Borba-Santos et al., 2022; Di Marco et al., 2021; Dos Santos et al., 2022; Mahalapbutr et al., 2022). Our recent studies have demonstrated the in vitro and in silico anticancer activities of brominated PQ analogs against MCF7 breast cancer cells *via* cell cycle arrest and oxidative stress induction (Jannuzzi et al., 2022). This was followed by another report claiming the anticancer potential of chlorinated PQ analogs against the MCF7 cell line *via* oxidative stress, apoptosis, and the suppression of cell proliferation (Jannuzzi et al., 2021). Encouraged by these results, our study was conducted with non-halogenated PQ analogs as a model substrate for treating colorectal cancer by performing in vitro and in silico studies (Ciftci, Sever, Ocak, et al., 2022). We also showed strong action toward the two cell lines (HCT-116 and

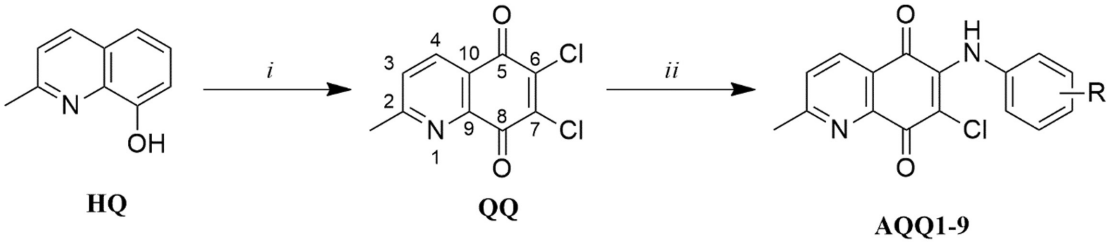

(i) $NaClO_3$, HCl, 50-60°C; (ii) $CeCl_3.7H_2O$, corresponding aryl amines, EtOH, rt to reflux, 3-6 h.

ID	R	ID	R	ID	R
AQQ1	2-$COOCH_3$	**AQQ4**	2-$COOCH_2CH_3$	**AQQ7**	2-$COOC(CH_3)_3$
AQQ2	3-$COOCH_3$	**AQQ5**	3-$COOCH_2CH_3$	**AQQ8**	3-$COOC(CH_3)_3$
AQQ3	4-$COOCH_3$	**AQQ6**	4-$COOCH_2CH_3$	**AQQ9**	4-$COOC(CH_3)_3$

SCHEME 1 Regioselective preparation of the aminated QQs (**AQQ1-9**).

MCF7) with enhanced apoptosis in both cell lines (Ciftci, Sever, Bayrak, et al., 2022). Our research group followed the 1,4-quinone moiety as a main part condensed with pyridine, named quinolinequinones, for cancer research, including its potential in the drug discovery field, and, last but not least, its potential impact in the field of monitoring response and toxicity to different cancer cell lines. The freshly obtained results for MCF7 and T-47D cells from luminal type A breast tumors were clearly meaningful; in both cell lines, quinolinequinone promoted ROS generation and apoptosis and dose-dependently decreased colony formation (Yilmaz Goler et al., 2022). Herein, testing the nine aminated QQs against the NCI panel of 60 cell lines will provide comprehensive information on the growth inhibitory effects of QQ analogs.

The single-dose findings for each of the tested AQQ analogs are presented in Table 1 as a mean graph of the cell **G**rowth **P**ercentage (GP). The percentage of **G**rowth **I**nhibition (GI%) (values between 0 and 100) and lethality (values less than 0) were determined as the percentage of in vitro growth inhibition and lethality, respectively. The results of each tested quinolinequinone are discussed within the text in terms of percent growth inhibition and were calculated by subtracting GP from hundred (GI% = 100 − GP) (Ciftci et al., 2019; Cuartas et al., 2021). Among all QQs, two (**AQQ1** and **AQQ4**) were found to be ineffective against all cancer cell lines. This is consistent with the results of our previous studies (Bayrak et al., 2020; Ciftci et al., 2019; Kara et al., 2020). The QQs showed the most notable anticancer activity against leukemia cancer cell lines. None of the quinolinequiones had acceptable inhibitory effects on a few cancer cell lines such as non-small cell lung cancer (except for EKVX and NCI-H522), CNS cancer, renal cancer (except for ACHN and UO-31), and prostate cancer cell lines. Regarding the two types of non-small cell lung cancer, the EKVX cancer cell line showed powerful sensitivity to **AQQ7** with GI% = 72.01, and the NCI-H522 cancer cell line exhibited remarkable sensitivity to **AQQ6** with GI% = 75.90. **AQQ2** was found to be the most active quinolinequinone in the ACHN renal cancer cell line (GI% 99.57). AQQ3 is another quinolinequinone-sensitive molecule in ACHN cells. **AQQ6** was the most active quinolinequinone in this series, possessing powerful activity against the UO-31 cell line (GI% = 97.63). Ovarian IGROV1, OVCAR-3, and NCI/ADR-RES cell lines were sensitive to six AQQs with a GI% range of 62.53–98.56. Three quinolinequinones (**AQQ2**, **AQQ8**, and **AQQ9**) were the most potent quinolinequinones among all tested quinolinequinones against OVCAR-3 (GI% 95.80, 62.53, and 98.56, respectively). Different types of the colon (HCT-116, HCT-15, HT29, and SW-620) and melanoma cell lines (LOX IMVI, MALME-3 M, MDA-MB-435, SK-MEL-28, and UACC-257) were shown to be susceptible to some of the quinolinequinones (GI% = 65.41–99.96). The most active quinolinequinone in this series was **AQQ2,** with a GI of % 99.96 against colon cancer (SW-620). Two colon cancer cell lines (HCT-116 and SW-620) were found to be the most sensitive to quinolinequinones. **AQQ6** possessed excellent potency and showed the best activity against the LOX IMVI cell line, with a GI% of 99.75. Finally, breast MCF7, BT-549, and T-47D cell lines showed good sensitivity (GI% = 61.43–88.66). While **AQQ9** was the most active in this series against the MCF7 cell line (GI% = 88.66), **AQQ3** possessed potent activity against the T-47D cell line (GI% = 68.84).

3.2.2 | In vitro full panel five-dose 60-cell lines assay

Based on the in vitro single-dose anticancer screening results of the tested quinolinequinones, **AQQ2**, **AQQ6**, **AQQ7**, and **AQQ9** were selected as lead quinolinequinones because of their pronounced anticancer selectivity compared with the rest of the quinolinequinones for evaluation in the full panel five-dose in vitro anticancer screening at 10-fold dilutions in the range of 0.01–100 μM. To establish dose–response curves and determine the biological potential of the tested quinolinequinones, three essential parameters (indicative concentration at which 50% of growth inhibitory activity [GI_{50}], indicative concentration at which 50% of cancer cells were killed [LC_{50}], and total growth inhibition [TGI]) were calculated for each cell line from log concentration versus % growth inhibition curves for nine panels of human cancer cell lines (Boyd & Paull, 1995; Monks et al., 1991). However, **AQQ9** does not exhibit adequate anticancer activity. Table 2 lists the outcomes of the selected quinolinequinones' in vitro anticancer five-dose screening in terms of three response parameters, including GI_{50}, TGI, and LC_{50} in μM.

Among the selected quinolinequinones (**AQQ2**, **AQQ6**, **AQQ7**, and **AQQ9**), **AQQ7** showed remarkable anticancer activity against all leukemia cell lines with GI_{50} values in the range of 0.394–1.78 μM. With regard to sensitivity against individual cell lines, **AQQ7** was found to be highly sensitive against all leukemia cell lines, non-small cell lung cancer EKVX (GI_{50} = 1.59 μM), HOP-92 (GI_{50} = 1.53 μM), and NCI-H522 (GI_{50} = 1.83 μM), colon cancer COLO 205 (GI_{50} = 1.77 μM), HCC-2998 (GI_{50} = 1.75 μM), HCT-116 (GI_{50} = 1.61 μM), HCT-15 (GI_{50} = 1.37 μM), and SW-620 (GI_{50} = 1.84 μM), CNS cancer SF-539 (GI_{50} = 1.70 μM), most of the cell lines of melanoma in the range of 1.02–1.82 μM, ovarian cancer IGROV1 (GI_{50} = 1.73 μM), OVCAR-3 (GI_{50} = 1.31 μM), and OVCAR-4 (GI_{50} = 1.40 μM), most of the cell lines of renal cancer in the range of 1.42–1.93 μM, prostate cancer PC-3 (GI_{50} = 1.78 μM) and DU-145

TABLE 1 Percentage cell growth of quinolinequinones against 60 human cancer cell lines at 10 μM concentration (**AQQ1-9**).

Cancer cell lines		AQQ1	AQQ 2	AQQ 3	AQQ 4	AQQ 5	AQQ 6	AQQ 7	AQQ 8	AQQ 9
Mean growth (%)		96.14	63.06	67.49	99.31	85.94	45.12	14.41	76.96	46.42
Leukemia										
GP	CCRF-CEM	62.48	5.63	16.09	84.29	15.00	6.88	−27.09	10.57	−23.24
	HL-60 (TB)	74.70	24.33	21.17	70.89	42.05	47.47	−32.73	16.71	4.87
	K-562	86.99	6.34	7.53	89.59	15.56	7.29	−15.67	−18.11	0.66
	MOLT-4	79.68	19.68	19.77	84.81	48.48	16.26	−32.59	6.09	−6.96
	RPMI-8226	94.64	3.31	36.88	99.26	53.26	4.69	−31.82	28.01	−0.46
	SR	102.75	18.74	22.26	102.36	37.09	22.63	−30.82	5.81	−11.55
Non-small-cell lung cancer										
GP	A549/ATCC	98.01	102.13	94.08	107.27	100.94	94.26	102.05	105.62	99.86
	EKVX	88.14	54.30	76.61	95.06	92.12	68.39	27.99	86.30	76.50
	HOP-62	81.81	113.00	96.80	101.74	112.43	112.76	95.31	108.46	105.71
	HOP-92	120.13	120.64	141.89	117.52	107.83	102.68	−72.04	88.85	−54.89
	NCI-H226	93.74	86.97	81.32	100.40	89.49	85.54	74.93	82.79	85.80
	NCI-H23	77.46	53.07	54.75	81.50	65.21	52.00	10.56	73.74	75.18
	NCI-H322M	100.78	103.06	101.14	100.62	103.61	96.74	98.72	111.73	100.89
	NCI-H460	99.42	100.57	92.29	99.80	99.97	79.27	86.21	101.46	101.62
	NCI-H522	88.79	65.06	59.64	101.73	88.41	24.10	−33.78	60.57	−14.14
Colon cancer										
GP	COLO 205	113.11	115.59	111.11	120.04	119.50	58.85	−66.13	118.68	−46.13
	HCC-2998	101.95	104.73	101.59	97.25	122.20	80.28	92.30	112.57	103.24
	HCT-116	86.27	27.17	43.09	99.12	76.67	7.29	−84.65	14.03	−70.47
	HCT-15	90.49	51.55	22.67	91.73	72.20	−48.53	−66.24	47.09	−43.91
	HT29	106.51	110.35	90.47	112.13	115.96	71.47	26.17	114.26	100.44
	KM12	104.00	106.29	50.32	104.96	104.89	50.83	99.10	99.22	104.56
	SW-620	88.75	0.04	18.27	94.85	84.27	−19.64	−28.33	64.29	−42.02
CNS cancer										
GP	SF-268	95.64	99.55	72.87	99.22	96.17	70.79	79.57	93.37	87.64
	SF-295	105.73	106.58	61.35	110.08	112.98	65.04	91.77	103.52	104.40
	SF-539	103.49	111.48	72.57	96.15	104.42	54.32	83.14	104.88	99.97
	SNB-19	101.19	92.17	61.92	92.84	90.82	68.08	80.38	97.56	83.80
	SNB-75	80.75	118.60	106.19	81.05	108.39	70.08	98.57	95.71	83.83
	U251	100.98	105.67	46.85	104.19	102.80	63.77	71.53	88.47	83.50
Melanoma										
GP	LOX IMVI	88.76	10.19	45.11	98.75	65.14	0.75	−72.49	8.98	−59.33
	MALME-3 M	105.91	87.50	74.74	106.76	96.29	11.67	−45.93	126.65	24.02
	M14	104.02	98.28	59.87	108.51	96.38	52.37	−10.59	96.54	61.30
	MDA-MB-435	113.56	−38.59	60.59	111.43	107.86	21.62	84.67	97.91	87.64
	SK-MEL-2	101.22	100.72	88.29	112.35	104.73	78.21	93.56	114.60	115.57
	SK-MEL-28	110.18	93.61	75.42	106.99	103.39	55.18	34.59	102.64	82.52
	SK-MEL-5	98.48	97.90	68.35	99.88	98.22	63.58	45.30	88.05	87.61
	UACC-257	89.66	62.04	78.13	99.25	82.05	44.15	−63.48	72.27	29.53
	UACC-62	97.46	95.38	68.49	95.04	95.78	55.50	79.01	90.72	87.08

TABLE 1 (Continued)

Cancer cell lines		AQQ1	AQQ 2	AQQ 3	AQQ 4	AQQ 5	AQQ 6	AQQ 7	AQQ 8	AQQ 9
Ovarian cancer										
GP	IGROV1	71.40	−58.10	41.40	91.40	17.29	7.95	59.57	88.22	84.79
	OVCAR-3	63.80	4.20	63.56	90.60	46.07	−18.78	−63.59	37.47	1.44
	OVCAR-4	80.24	−97.60	58.53	83.60	53.67	−62.72	−45.32	65.67	42.67
	OVCAR-5	99.71	99.79	105.06	101.31	103.95	91.55	138.92	129.73	127.21
	OVCAR-8	96.95	77.38	70.10	100.26	97.79	68.43	66.76	87.32	80.28
	NCI/ ADR-RES	88.67	89.74	19.69	93.91	94.64	45.92	64.16	93.87	84.89
	SK-OV-3	87.12	87.62	125.16	108.39	98.05	94.36	105.12	97.22	100.51
Renal cancer										
GP	786–0	103.09	98.17	85.74	104.28	102.97	55.46	−79.17	99.81	−56.35
	A498	122.25	71.02	77.92	87.40	88.76	68.26	92.28	66.55	110.48
	ACHN	94.79	0.43	35.10	100.71	96.13	−9.88	−73.57	76.97	−21.52
	CAKI-1	94.71	102.98	80.23	98.60	108.02	75.38	−92.35	77.74	−34.79
	RXF 393	99.04	59.65	89.71	102.02	97.78	45.63	−81.72	84.31	−19.33
	SN12C	96.75	93.08	77.02	88.22	95.49	75.82	52.58	94.09	87.96
	TK-10	172.16	128.01	152.09	147.46	119.29	99.43	−84.59	120.25	83.91
	UO-31	82.39	48.52	61.73	91.87	93.07	2.37	−62.69	78.42	46.40
Prostate cancer										
GP	PC-3	94.05	85.39	57.30	96.76	81.99	48.03	67.08	72.02	72.14
	DU-145	108.15	104.66	68.55	111.60	108.12	90.97	−56.25	94.81	97.94
Breast cancer										
GP	MCF7	83.88	−35.25	30.46	87.47	75.97	−14.46	−60.10	53.26	11.34
	MDA-MB-231/ ATCC	76.54	62.60	91.87	90.30	89.79	77.43	55.50	74.39	53.94
	HS 578 T	99.49	102.32	71.52	99.03	111.00	50.16	84.09	101.86	100.96
	BT-549	118.63	124.81	98.98	114.14	121.11	NT	38.57	101.52	83.99
	T-47D	95.64	−28.12	31.16	92.82	56.35	−0.93	−25.16	59.09	−8.23
	MDA-MB-468	101.52	−71.34	55.95	97.27	−33.42	−24.63	−76.50	−57.68	−50.30

Abbreviation: NT, not tested.

(GI_{50} = 1.77 μM), most of the cell lines of breast cancer in the range of 0.813–1.84 μM. **AQQ7** also exhibited superior cytotoxic activity against some leukemia cell lines (HL-60 (TB), RPMI-8226, and SR cell lines with TGI ranging from 1.90 to 7.86 μM), most colon, ovarian, renal, and all prostate and breast cancer cell lines with TGI ≤10 μM. In contrast, LC_{50} values were greater than 100 μM against the entire panel of leukemia cell lines. Other good cytotoxicities were recorded against EKVX, HOP-92, and NCI-H522 (non-small cell lung cancer), COLO 205, HCC-2998, HCT-116, HCT-15, and SW-620 (colon cancer), SF-539 (CNS cancer), all melanoma cell lines except that SK-MEL-2, IGROV1, OVCAR-3, and OVCAR-4 (ovarian cancer), all renal cancer cell lines except that A498, all prostate cancer cell lines, and MCF7, MDA-MB-231/ATCC, T-47D, and MDA-MB-468 (breast cancer) were noticed with most of the sensitive cell lines. **AQQ7** showed potent lethal action against most cell lines, except for some leukemia, colon, CNS, ovarian, and breast cancer cell lines. Figure 1 shows all **AQQ7** five dose–response curves against the 60 human cancer cell line panel. In addition, **AQQ6** was identified as the lead molecule against K-562 and SR leukemia cell lines, with GI_{50} values of 0.371 and 0.783 μM, respectively. Furthermore, this quinolinequinone demonstrated notable anticancer activity against some of the colon, melanoma, ovarian, renal, prostate, and breast cancer cell lines with GI_{50} values ranging from 1.53 to 2.10 μM as shown in (Table 2). **AQQ6** exhibited significant TGI values ranging from 3.01 to 10.80 μM in most of the tested cell lines. LC_{50} values >100 μM were observed in all leukemia cell lines, except the HL-60 (TB) cell line. **AQQ6** has demonstrated excellent anticancer activity against several colon cancer

TABLE 2 GI_{50}, TGI, and LC_{50} values (μM) of anticancer activity data as per the five-dose assay of the selected quinolinequinones (**AQQ2**, **AQQ6**, **AQQ7**, and **AQQ9**) after 48 h based on the SRB assay at the NCI.

Molecule	AQQ2 (NCI: D-827044/1)			AQQ6 (NCI: D-827043/1)			AQQ7 (NCI: D-827611/1)			AQQ9 (NCI: D-827609/1)		
Panel/cell line	**GI_{50}**	**TGI**	**LC_{50}**	**GI_{50}**	**TGI**	**LC_{50}**	**GI_{50}**	**TGI**	**LC_{50}**	**GI_{50}**	**TGI**	**LC_{50}**
Leukemia												
CCRF-CEM	2.01	5.48	>100	1.27	4.88	>100	0.425	>100	>100	5.90	>92.5	>92.5
HL-60 (TB)	1.53	3.64	8.67	1.10	3.21	9.35	0.394	1.90	>100	7.65	71.1	>92.5
K-562	0.976	3.94	>100	0.371	3.30	>100	0.549	>100	>100	3.77	>92.5	>92.5
MOLT-4	2.53	5.68	>100	1.57	5.33	>100	0.705	ND	>100	4.65	72.8	>92.5
RPMI-8226	2.14	6.00	>100	2.16	5.95	>100	1.78	5.90	>100	23.3	>92.5	>92.5
SR	1.83	4.62	>100	0.783	3.57	>100	0.442	7.86	>100	3.44	55.7	>92.5
Non-small-cell lung cancer												
A549/ATCC	18.1	37.9	79.0	19.4	70.5	>100	44.5	>100	>100	>92.5	>92.5	>92.5
EKVX	1.77	3.60	7.34	2.53	7.55	71.5	1.59	3.01	5.67	>92.5	>92.5	>92.5
HOP-62	15.1	29.6	58.1	10.2	23.9	55.8	3.59	18.3	95.3	>92.5	>92.5	>92.5
HOP-92	1.92	3.95	8.11	1.80	3.48	6.73	1.53	2.89	5.49	16.4	36.7	82.1
NCI-H226	2.02	4.39	9.54	3.43	17.5	99.7	6.77	>100	>100	>92.5	>92.5	>92.5
NCI-H23	1.82	4.08	ND	2.31	7.57	52.7	NT	NT	NT	NT	NT	NT
NCI-H322M	16.0	30.3	57.5	16.7	33.0	65.6	10.7	54.0	>100	>92.5	>92.5	>92.5
NCI-H460	18.5	41.5	93.2	8.76	30.1	97.0	3.08	11.3	67.6	>92.5	>92.5	>92.5
NCI-H522	1.89	4.46	>100	1.71	3.72	8.08	1.83	3.86	8.13	16.3	35.7	78.2
Colon cancer												
COLO 205	1.77	3.76	7.99	1.75	3.58	7.35	1.77	3.48	6.84	21.9	63.0	>92.5
HCC-2998	2.21	4.79	11.6	3.63	13.8	44.8	1.75	3.27	6.12	>92.5	>92.5	>92.5
HCT-116	1.60	3.32	6.88	1.87	4.36	>100	1.61	3.15	6.18	15.5	32.0	66.1
HCT-15	1.54	3.33	7.19	1.57	3.37	7.25	1.37	3.32	8.08	15.4	33.9	74.8
HT29	2.32	6.09	81.8	2.18	5.13	>100	2.94	8.52	>100	>92.5	>92.5	>92.5
KM12	13.3	29.4	64.8	3.37	12.9	65.4	6.07	50.4	>100	>92.5	>92.5	>92.5
SW-620	1.97	4.03	8.24	2.06	4.41	9.44	1.84	6.26	>100	18.5	44.0	>92.5
CNS cancer												
SF-268	2.76	9.59	97.1	3.86	17.1	73.2	3.06	14.7	92.5	>92.5	>92.5	>92.5
SF-295	15.8	29.9	56.6	5.48	19.1	50.8	4.25	22.5	>100	>92.5	>92.5	>92.5
SF-539	1.75	3.27	6.11	2.52	6.72	28.2	1.70	3.18	5.96	>92.5	>92.5	>92.5

TABLE 2 (Continued)

Molecule	AQQ2 (NCI: D-827044/1)			AQQ6 (NCI: D-827043/1)			AQQ7 (NCI: D-827611/1)			AQQ9 (NCI: D-827609/1)		
Panel/cell line	**GI_{50}**	**TGI**	**LC_{50}**	**GI_{50}**	**TGI**	**LC_{50}**	**GI_{50}**	**TGI**	**LC_{50}**	**GI_{50}**	**TGI**	**LC_{50}**
SNB-19	10.8	>100	>100	4.76	89.4	>100	3.30	15.4	>100	>92.5	>92.5	>92.5
SNB-75	13.2	26.2	52.2	2.30	10.3	35.4	14.7	>100	>100	>92.5	>92.5	>92.5
U251	3.27	11.8	42.4	3.75	16.1	50.4	2.42	6.81	33.9	>92.5	>92.5	>92.5
Melanoma												
LOX IMVI	1.68	3.64	ND	1.72	3.58	ND	1.02	2.31	5.25	16.9	33.0	64.3
MALME-3 M	1.95	3.76	7.24	1.83	3.62	7.17	1.66	3.27	6.46	15.7	30.5	59.0
M14	1.84	3.42	6.38	1.85	3.76	7.67	1.73	3.38	6.62	29.3	>92.5	>92.5
MDA-MB-435	2.04	4.29	9.00	3.21	10.8	43.2	1.71	3.19	5.97	90.3	>92.5	>92.5
SK-MEL-2	2.27	6.48	26.5	2.89	9.46	33.7	2.27	6.78	>100	>92.5	>92.5	>92.5
SK-MEL-28	1.96	3.71	7.04	2.47	6.02	23.8	1.66	3.12	5.88	18.2	38.5	81.5
SK-MEL-5	1.80	3.34	6.19	2.21	5.63	20.4	1.59	2.98	5.58	>92.5	>92.5	>92.5
UACC-257	1.57	3.00	5.72	1.63	3.12	5.97	1.69	3.3	6.45	31.6	>92.5	>92.5
UACC-62	2.62	8.10	>100	2.46	11.2	68.8	1.82	3.98	8.71	>92.5	>92.5	>92.5
Ovarian cancer												
IGROV1	1.98	3.89	7.62	3.43	11.3	48.8	1.73	3.43	6.79	71.4	>92.5	>92.5
OVCAR-3	1.59	3.03	5.78	1.78	3.22	5.86	1.31	2.96	6.72	13.8	30.4	66.9
OVCAR-4	1.42	2.89	5.88	1.67	3.26	6.37	1.40	2.78	5.53	12.7	29.2	67.1
OVCAR-5	3.14	14.7	75.3	13.2	33.7	85.6	2.05	4.10	8.17	>92.5	>92.5	>92.5
OVCAR-8	1.78	3.44	ND	4.38	18.4	61.6	2.83	9.32	>100	>92.5	>92.5	>92.5
NCI/ADR-RES	2.25	6.28	>100	2.57	9.61	60.6	2.17	5.35	>100	>92.5	>92.5	>92.5
SK-OV-3	12.5	25.2	51.0	10.5	23.9	54.4	>100	>100	>100	>92.5	>92.5	>92.5
Renal cancer												
786-0	1.86	3.66	7.18	1.88	3.93	8.21	1.69	3.22	6.15	>92.5	>92.5	>92.5
A498	12.0	24.6	50.6	11.7	28.3	68.6	12.4	47.8	>100	>92.5	>92.5	>92.5
ACHN	1.78	3.40	6.48	1.81	3.35	6.18	1.75	3.14	5.62	15.8	28.6	51.6
CAKI-1	1.71	3.28	6.29	1.53	2.99	5.86	1.55	2.90	5.43	14.4	30.6	64.8
RXF 393	1.57	2.94	5.52	1.63	3.02	5.60	1.62	2.99	5.51	12.8	25.5	51.0
SN12C	2.13	5.40	>100	3.51	20.2	>100	1.93	4.22	ND	>92.5	>92.5	>92.5
TK-10	1.78	3.19	5.72	1.79	3.24	5.86	1.81	3.28	5.93	>92.5	>92.5	>92.5
UO-31	1.44	2.79	5.42	1.54	3.01	5.88	1.42	2.74	5.28	18.9	53.1	>92.5

(Continues)

TABLE 2 (Continued)

Molecule	AQQ2 (NCI: D-827044/1)			AQQ6 (NCI: D-827043/1)			AQQ7 (NCI: D-827611/1)			AQQ9 (NCI: D-827609/1)		
Panel/cell line	GI_{50}	TGI	LC_{50}	GI_{50}	TGI	LC_{50}	GI_{50}	TGI	LC_{50}	GI_{50}	TGI	LC_{50}
Prostate cancer												
PC-3	2.80	10.3	80.6	3.31	15.7	57.4	1.78	4.19	9.86	>92.5	>92.5	>92.5
DU-145	1.86	3.39	6.17	1.82	3.40	6.36	1.77	3.32	6.21	>92.5	>92.5	>92.5
Breast cancer												
MCF7	1.89	4.61	26.5	1.88	4.32	ND	0.813	3.58	>100	16.0	35.3	77.7
MDA-MB-231/ATCC	2.15	5.08	>100	3.73	17.1	>100	1.58	3.26	6.76	30.2	>92.5	>92.5
HS 578 T	2.46	6.26	>100	2.55	7.00	>100	2.39	7.54	>100	>92.5	>92.5	>92.5
BT-549	1.68	3.09	5.67	2.06	5.10	16.6	2.90	9.04	49.0	>92.5	>92.5	>92.5
T-47D	2.04	5.02	>100	2.10	5.09	>100	1.84	4.91	>100	16.6	55.4	>92.5
MDA-MB-468	1.61	3.28	6.68	1.66	3.54	7.56	1.47	3.25	7.16	11.1	26.7	64.1

Abbreviations: ND, not determined; NT, not tested.

cell lines (COLO 205 and HCT-116). **AQQ2** showed the highest anticancer activity against K-562 leukemia cell line (GI_{50} = 0.976 μM). Quinolinequinone demonstrated significant anticancer activity against most of the tested cancer cell lines, with GI_{50} values ranging from 0.976 to 2.62 μM. The TGI values ranged from 2.79 to 10.30 μM. Finally, diminished lethality (LC_{50} values >100 μM) was observed in all leukemia cell lines except the HL-60 (TB) cell line and most of the breast cancer cell lines.

3.2.3 | Cytotoxic evaluation of **AQQ2** and **AQQ7** with MTT assay

According to the MTT assay results, **AQQ7** showed greater cytotoxic activity than that of **AQQ2**. Especially, IC_{50} values were as low as 2.08 ± 0.27 and 3.34 ± 0.37 μM for MCF7 and T-47D breast cancer cells, respectively. Positive control drug ADRI IC_{50} concentration was 14.16 ± 1.55 μM in MCF7 cells and 5.50 ± 1.25 μM in non-cancerous HaCaT cells, indicating poor selectivity. On the contrary, **AQQ7** IC_{50} for HaCaT cells was 2.50 ± 0.16 μM, which is higher than the promising IC_{50} value of MCF7 cells (2.08 ± 0.27 μM). Additionally, both **AQQ2** and **AQQ7** showed higher cytotoxic activity than ADRI in COLO 205 colon cancer cells, supporting the anticancer potential of **AQQ2** and **AQQ7** (Figure 2; Table 3).

3.2.4 | Apoptotic and necrotic effects of **AQQ7**

Thus, **AQQ7** was further investigated in MCF7 cells. For this purpose, 0.5, 1, and 2.5 μM **AQQ7** were applied to MCF7 cells for 24 h. Next, we examined the effects of **AQQ7** on the cell death pathways of MCF7 cells using dual Annexin V/PI staining by flow cytometry. Although an increasing apoptosis trend was detected in the **AQQ7**-treated groups compared to the control, it was statistically significant at the 2.5 μM **AQQ7** concentration (Figure 3). In contrast, 2.5 μM ADRI as a positive control significantly reduced the live cell population and increased apoptosis. The apoptotic activity of the quinolinequinone moiety was demonstrated previously by different groups and in our previous studies (Ambrose et al., 2005; Bayrak et al., 2021).

3.2.5 | Effects of **AQQ7** on cell cycle progression

The effects of **AQQ7** on cell cycle phases were examined. Although the cell populations in the G0/G1 phase showed a slight decrease and those in the S phase slightly increased

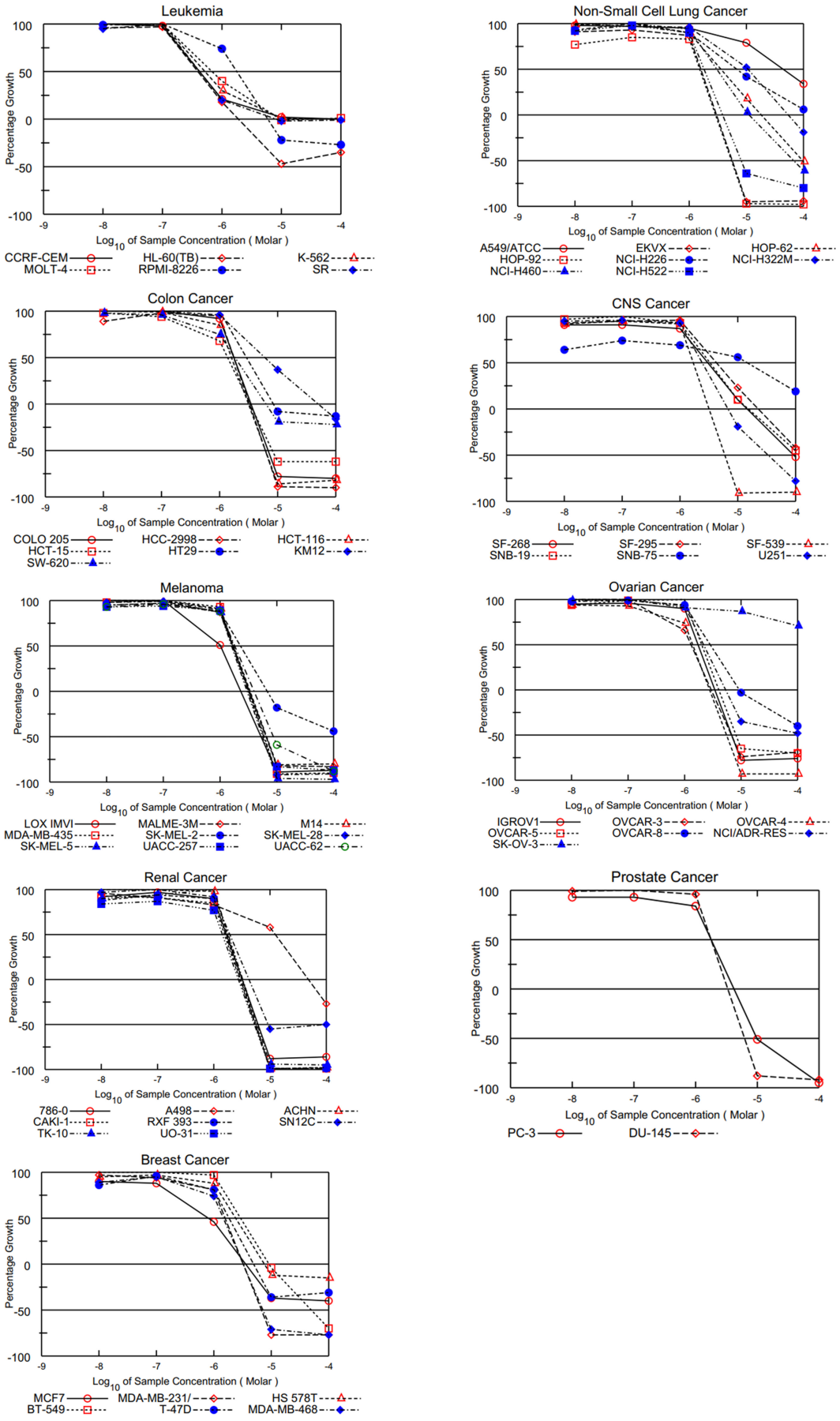

FIGURE 1 Graphical presentation of growth inhibition by **AQQ7** at five dose concentrations after 48 h based on the SRB assay at NCI.

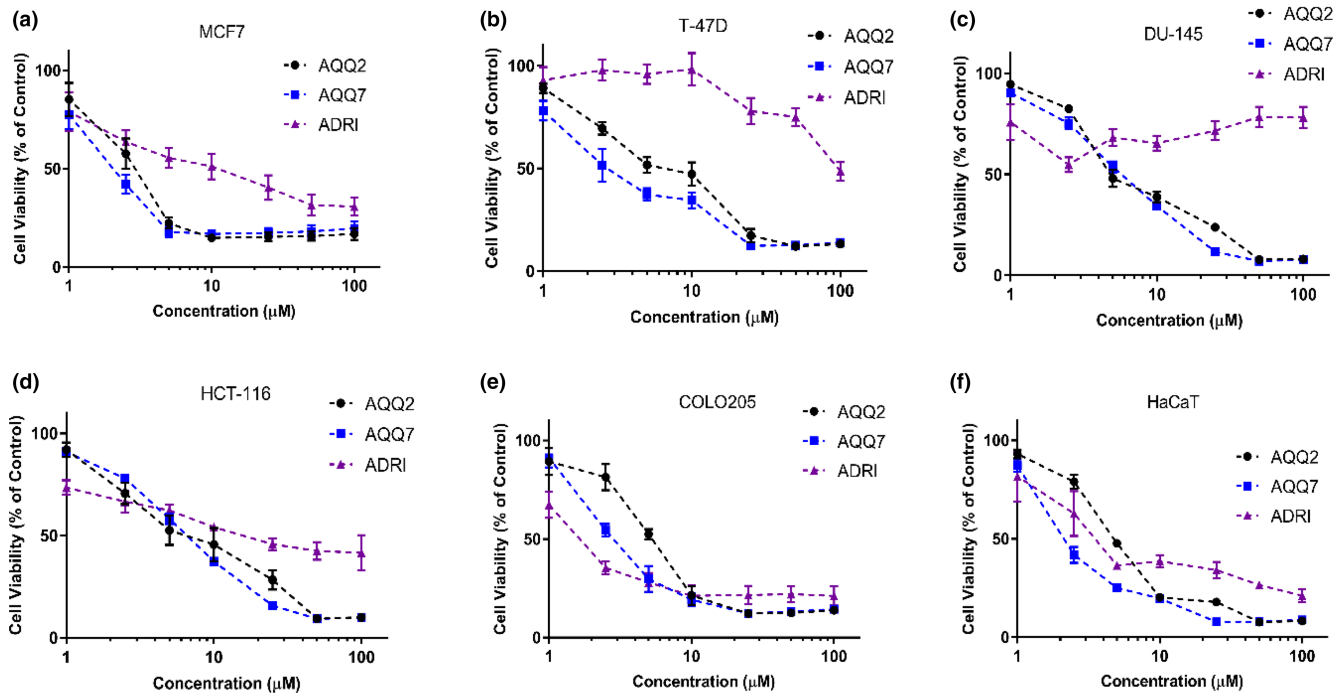

FIGURE 2 The cytotoxic activities of **AQQ2** and **AQQ7** in MCF7 and T-47D breast cancer, DU-145 prostate cancer, HCT-116, and COLO 205 colon cancer cell lines were determined by MTT assay after 24 h of exposure. HaCaT human keratinocytes were used as a non-cancerous cell line, and adriamycin (ADRI) was used as a positive control. Values are expressed as the mean ± SEM.

TABLE 3 IC_{50} concentrations of **AQQ2** and **AQQ7** in MCF7 and T-47D breast cancer, DU-145 prostate cancer, HCT-116, and COLO 205 colon cancer cell lines.

(μM)	MCF7	T-47D	DU-145	HCT-116	COLO 205	HaCaT
AQQ2	2.89 ± 0.24	6.61 ± 0.50	6.73 ± 0.39	7.21 ± 0.78	5.40 ± 0.44	5.08 ± 0.25
AQQ7	2.08 ± 0.27	3.34 ± 0.37	5.82 ± 0.21	6.72 ± 0.22	3.20 ± 0.28	2.50 ± 0.16
ADRI	14.16 ± 1.55	>100	>100	21.33 ± 4.85	1.41 ± 0.44	5.50 ± 1.25

Note: HaCaT human keratinocytes were used as a non-cancerous cell line, and ADRI was used as a positive control. Values are expressed as the mean ± SEM.

with **AQQ7** treatment, there was no significant difference in the applied concentrations of **AQQ7** compared to the control (Figure 4). The positive control drug ADRI caused a significant increase in the cell population in the S and G2 + M phases. These results suggested that the cell cycle does not play an important role in the anticancer effect of **AQQ7**.

3.2.6 | Effects of **AQQ7** on oxidative stress

Overproduction of reactive oxygen species (ROS) induces oxidative stress and contributes to anticancer therapy (Kim et al., 2019). The ability of **AQQ7** to generate intracellular ROS was evaluated using flow cytometry. There was no significant difference in the amount of intracellular ROS between **AQQ7**-treated and control groups (Figure 5).

Because of the promising results obtained from molecular anticancer studies of quinolinequinones in recent years, these molecules have attracted the attention of an increasing number of researchers. Many efforts have been made to strengthen their anticancer effects and increase cancer selectivity by exploring newly synthesized derivatives. Our group has established and characterized several compounds with quinolinequinone moieties to develop novel anticancer drugs.

3.3 | In vitro ADME and in vivo pharmacokinetic profiling

AQQ2 was subjected to in vitro ADME profiling (Table 4) and in vivo pharmacokinetic (PK) profiling. During in vivo PK profiling, we could not quantify the compound in rat plasma samples because of the irregular profiles near

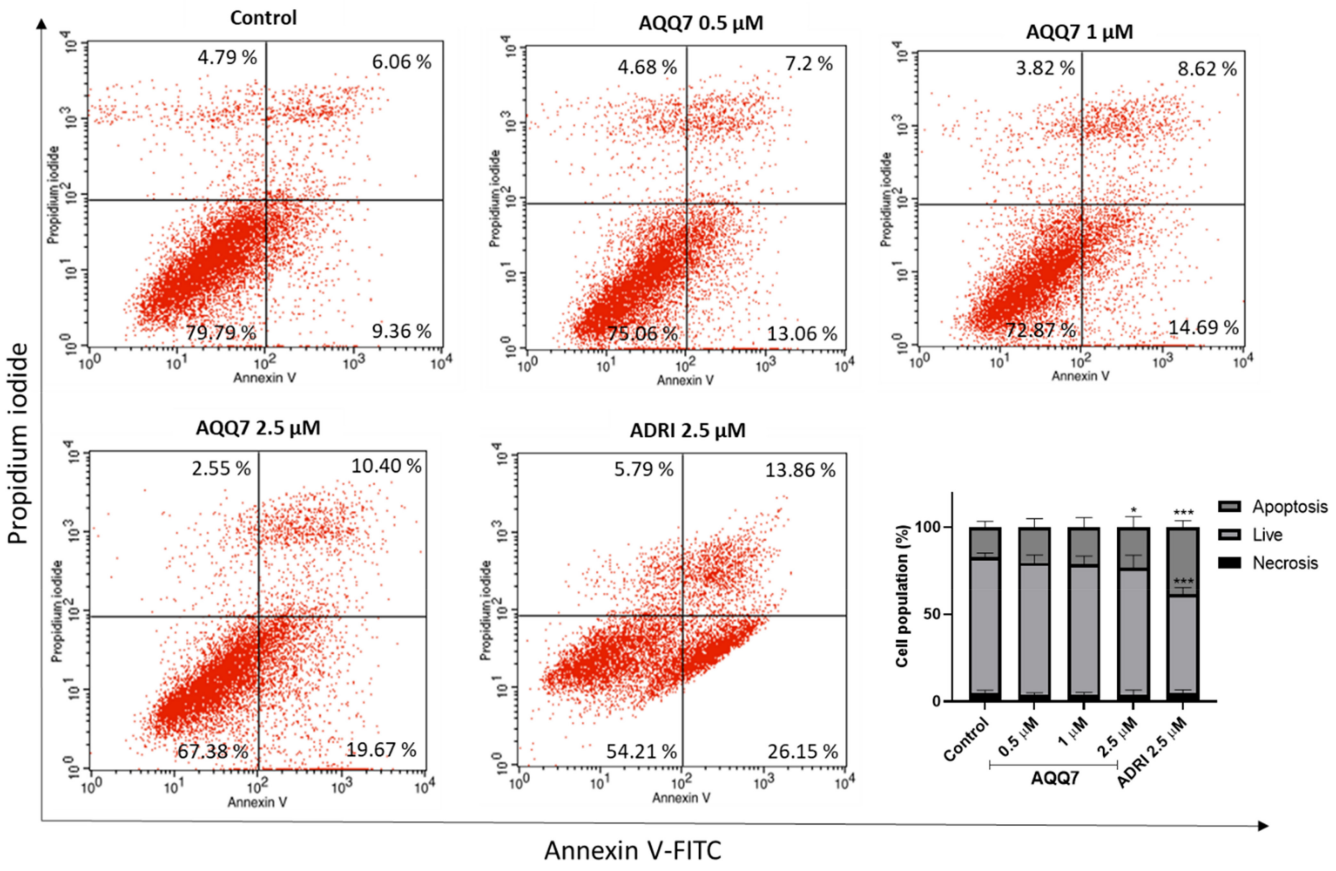

FIGURE 3 **AQQ7**-induced apoptosis and necrosis were determined using Annexin V-FITC/PI double staining by flow cytometry in MCF7 cells. Cells were classified as live cells (Annexin V^-, PI^-), apoptotic cells (Annexin V^+, PI^- and Annexin V^+, PI^+), and necrotic cells (Annexin V^-, PI^+). Representative images and quantitative results of apoptosis analysis using (A) representative flow cytometry plots. MCF7 cells. Plotted mean values of the assay results. Values are expressed as the mean ± SEM. (*$p < 0.05$, ***$p < 0.001$ compared to control).

the lowest calibration range. Because the compound did not degrade under ex vivo conditions, it was suggested that the compound might undergo rapid metabolism in vivo. In vitro metabolic stability study using rat liver microsomes has confirmed that nearly 93% of the drug gets metabolized within 30 min with a half-life of 7.5 min and CL_{int} of 183. The compound exhibited poor metabolic stability in human liver microsomes. In addition, ADMETLab2.0 predicted low permeability in both Caco-2 (−4.61) and MDCK (2.2×10^{-5}) models with poor oral bioavailability ($F_{20\%}$ of 0.001). Targeted delivery to the tumor environment may be useful for compounds of this type. Furthermore, a lead optimization strategy to improve permeability and metabolic stability through the chemical modification of **AQQ2** is under consideration.

3.4 | Molecular docking simulation

Molecular docking simulations were performed to identify the putative targets of **AQQ2** and **AQQ7**. As **AQQ2** and **AQQ7** have shown activity against breast, cervical, and prostate cancer cell lines, we selected three proteins: cyclooxygenase (COX, PDB:6BL4), phosphate and tensin homolog (PTEN, PDB:1D5R), and epidermal growth factor receptor (EGFR, PDB:1M17), which have been reported to be overexpressed in these cancers (Gonzalez-Conchas et al., 2018; Harris et al., 2014; Hirsch et al., 2003; Song et al., 2023). Table 5 summarizes the results of docking simulations. Both compounds displayed potent interactions with COX and EGFR with estimated Ki values in the sub-micromolar range, and their molecular-level interactions are discussed below.

We further analyzed the complexes of the three proteins using LigPlot+ and PLIP v2.2.2. Hydrophobic interactions are critical components of protein–ligand binding. In the case of COX, we identified the common residues involved in these interactions with **AQQ2** and **AQQ7**: VAL349, LEU352, SER353, TYR355, PHE381, LEU384, TYR385, TRP387, PHE518, MET522, VAL523, and GLY526. PLIP v2.2.2 analysis revealed the π-π stacking interaction of the side chain phenyl ring of **AQQ2** and **AQQ7** with TYR355

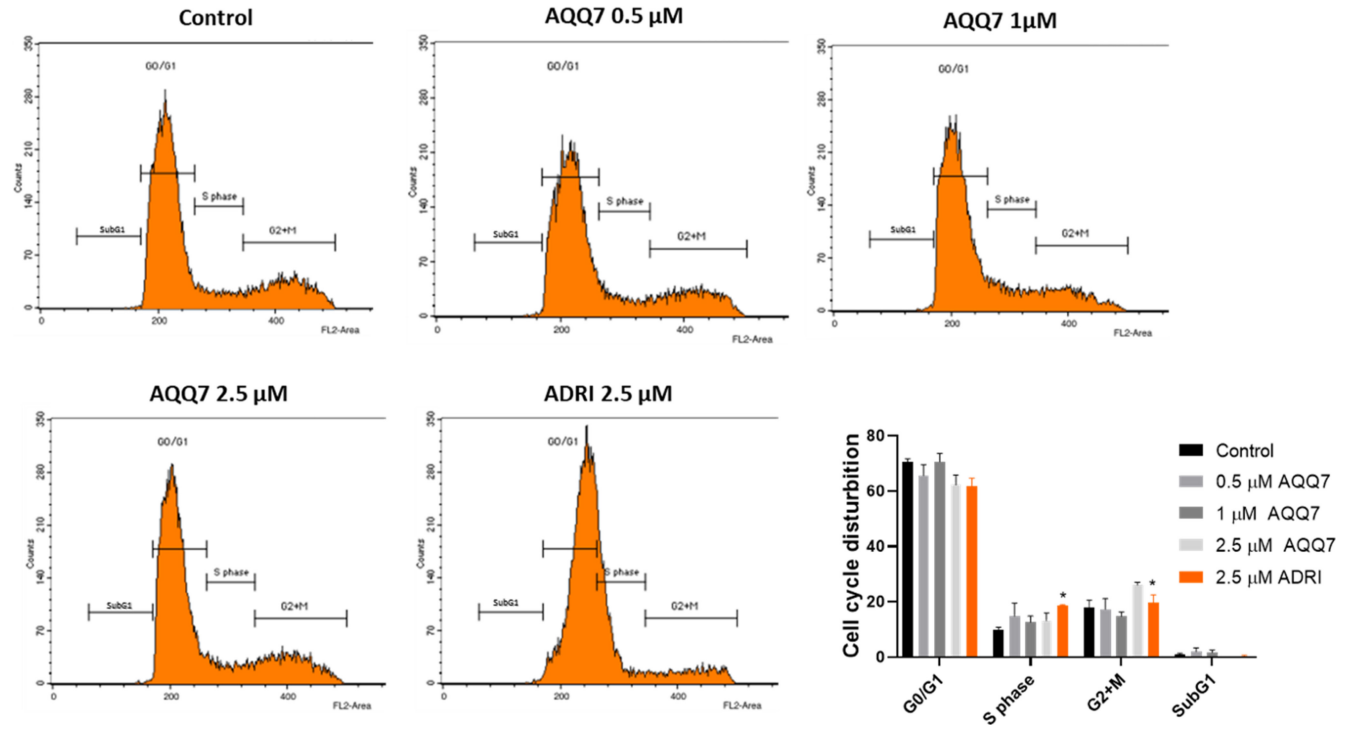

FIGURE 4 The effect of **AQQ7** on the progression of the MCF7 cell cycle was analyzed by flow cytometry. Representative cell cycle phase distribution histograms and quantitative results of cell cycle analysis. Plotted mean values of the assay results. Values are expressed as the mean ± SD. (*$p < 0.05$, compared with the control).

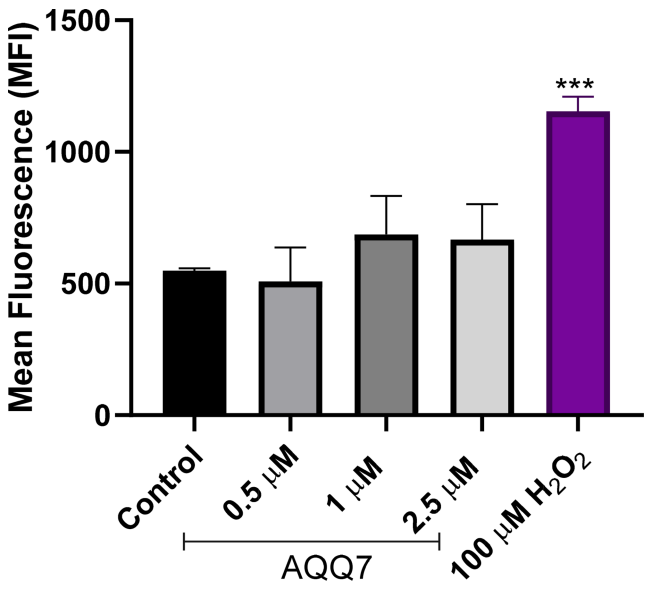

FIGURE 5 **AQQ7**-induced oxidative stress was determined by DCDFA staining using flow cytometry in MCF7 cells. Bar graphs of the quantitative results of ROS production analysis. The values expressed as mean ± SEM (***$p < 0.001$, compared to control).

and TRP387 (Figure 6). The position (meta) and less bulky (methyloxycarbloxy) of the substitution over the phenyl ring of **AQQ2** favor the establishment of H-bonding interactions between the carbonyl oxygen of quinone and the side chain phenolic -OH of Tyr385. **AQQ7** lacks this interaction but is compensated by the hydrophobic interaction in such a way that there is no significant difference in the estimated Ki values.

A similar 2D-interaction plot for **AQQ2** and **AQQ7** with EGRR (PDB: 1M17) is presented in Figure 7. Both compounds exhibited H-bonding interactions between the quinone oxygen and the backbone -NH of Met769. Thus, both compounds had similar pocket orientations, showing hydrophobic interactions with LEU694, VAL702, ALA719, LEU768, PRO770, GLY772, LEU820, and ASP831. **AQQ2** established additional H-bonding interactions between the carbonyl oxygen of the phenyl group and the side-chain–NH_2 group of LYS721. **AQQ7** did not show this interaction because of the position and bulkiness (t-butyloxycarbloxy) of the substitution over the phenyl ring. In this case, no significant difference was observed between the estimated Ki values of the two compounds.

In the case of PTEN, the hydrophobic interactions are characterized by a distance of 3.73 and 3.29 Å, respectively. Five residues, including LYS125, ALA126, ARG130, HIS93, and THR167, formed six hydrogen bonds with **AQQ2**, all interacting with the ligand's oxygen atom (O2) through their side chains, except for HIS93, which interacts through its main chain. The distances range from 2.11 to 3.2 Å, and the angles range from 142.36 to 160.72

degrees. The PLIP v2.2.2 analysis revealed a salt bridge between ARG130 and the carboxylate group of the ligand with a distance of 4.20 Å, a pi-cation interaction between HIS93 and the ligand's aromatic group with a distance of 4.64 Å and an offset of 1.13 Å, and a halogen interaction between GLN171 and the chlorine atom of the ligand (Cl) with a distance of 3.21 Å, a donor angle of 144.46 degrees, and an acceptor angle of 143.81 degrees. In **AQQ7**, one hydrogen bond was observed between GLY129 in chain A and the oxygen atom of **AQQ7**, with a distance of 3.02 Å. PLIP v2.2.2 analysis revealed two salt bridges, one between HIS93 in chain A and the carboxylate group of **AQQ7**, with a distance of 4.73 Å, and the other between LYS128 in chain A and the carboxylate group of **AQQ7**, with a distance of 4.31 Å (Figure 8).

TABLE 4 In vitro ADME profiling of compound **AQQ2**.

	AQQ2	Veerapamil	Atenolol
LogP[a]	1.93	−0.21	−0.33
LogD[a]	1.87	1.87	−1.77
Mouse liver microsomes			
%Metabolism in 30 min	86.5	80	
Half-life (min)	10	11	
CL_{int} (μL/min/mg protein)	144.5	130	
Rat liver microsomes			
%Metabolism in 30 min	93	79	
Half-life (min)	7.5	11	
CL_{int} (μL/min/mg protein)	183	121	
Dog liver microsomes			
%Metabolism in 30 min	90	81	
Half-life (min)	7.5	11	
CL_{int} (μL/min/mg protein)	191.5	131	
Human liver microsomes			
%Metabolism in 30 min	99	79	
Half-life (min)	3	11	
CL_{int} (μL/min/mg protein)	429	129	

[a]Partitioned toward *n*-octanol (lipophilic).

4 | CONCLUSIONS

The current study successfully illustrated the in vitro anticancer assessment of aminated quinolinequinones (**AQQ1-9**). These quinolinequinones were tested using the NCI 60 cell line panel to determine whether they could inhibit cell growth in various human tumor cell lines, including cell type-specific effects (Monks et al., 1991). Preliminary in vitro anticancer analysis suggested that aminated quinolinequinones (**AQQ1-9**) are the lead structures for cancer treatment, particularly against leukemia and breast cancer. The National Cancer Institute's one-dose experiment revealed distinct anticancer activity of four quinolinequinones (**AQQ2**, **AQQ6**, **AQQ7**, and **AQQ9**). To analyze the activity of quinolinequinones, an agent with a GI_{50} value of less than 1 μM is considered to be potent and potentially reflects selectivity toward that specific cancer cell line; as a result, this compound may be thought to have therapeutic potential for the treatment of such types of cancer. Thus, a super-sensitivity profile with low micromolar GI_{50}, TGI, and LC_{50} values against both panel cancer cell lines was observed for **AQQ7** against all leukemia cell lines (except for the RPMI-8226 cell line) and MCF7 breast cancer cell lines. In addition, using in vitro studies, we demonstrated that the MCF7 breast cancer cell line was the most sensitive to **AQQ7** among in vitro tested MCF7 and T-47D breast cancer, DU-145 prostate cancer, HCT-116, and COLO 205 colon cancer cell lines. **AQQ7** shows cytotoxic activity through the induction of apoptosis.

TABLE 5 Molecular docking simulation of **AQQ2** and **AQQ7** with COX, PTEN, and EGFR.

Code	Parameter	Cyclooxygenase (COX) PDB: 6BL4	Phosphatase and tensin homolog (PTEN) PDB: 1D5R	Epidermal growth factor receptor (EGFR) PDB: 1M17
AQQ2	Estimated free energy of binding (kcal/mol)	−9.98	−7.75	−8.38
	Estimated Ki (μM)	0.048	2.09	0.72
AQQ7	Estimated free energy of binding (kcal/mol)	−10.03	−6.54	−8.62
	Estimated Ki (μM)	0.044	16.08	0.48

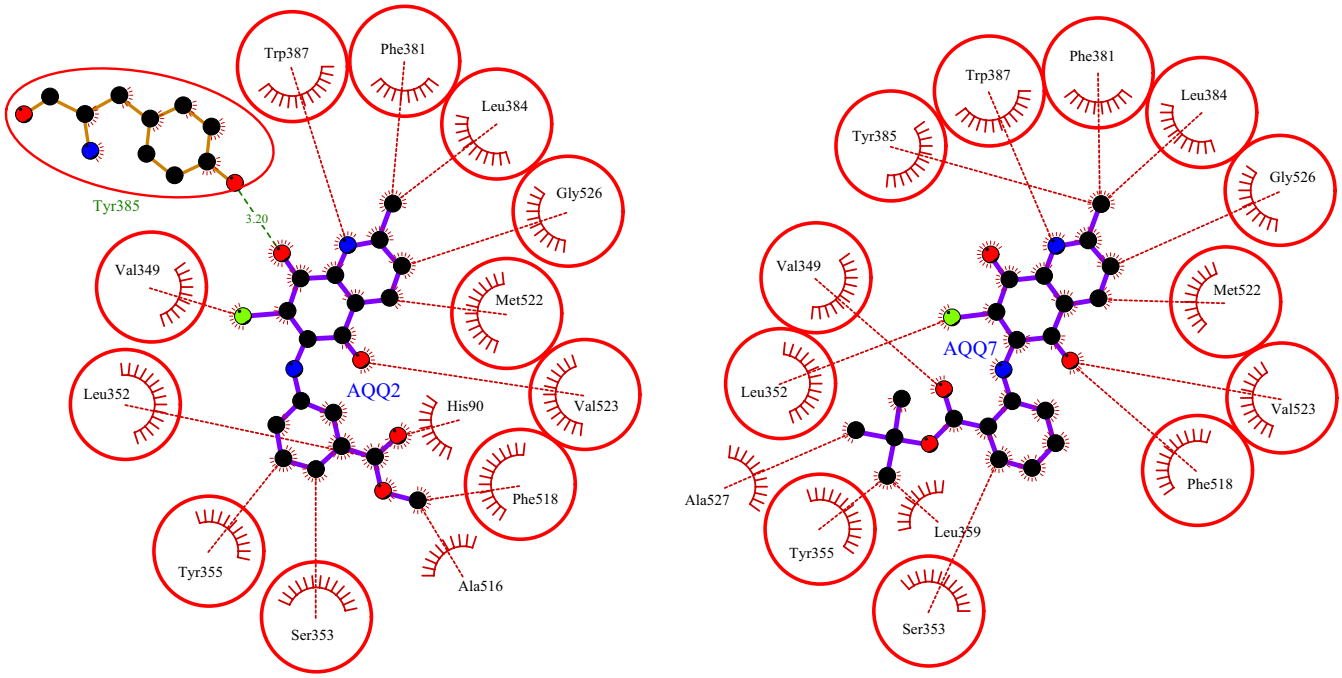

FIGURE 6 A 2D-interaction plot of **AQQ2** and **AQQ7** with COX (PDB: 6BL4). The interacting residues common to both ligands are indicated by red circles. Arcs with red spikes indicate hydrophobic residues, dashed red lines indicate representative hydrophobic interactions, and dashed green lines indicate H-bonding interactions. The atoms of the amino acid residues and ligands are colored by atom type (carbon: black, oxygen: red, nitrogen: blue, sulfur: yellow, and chloro: green); the bonds of the amino acid residues are colored brown; and the ligands are colored violet.

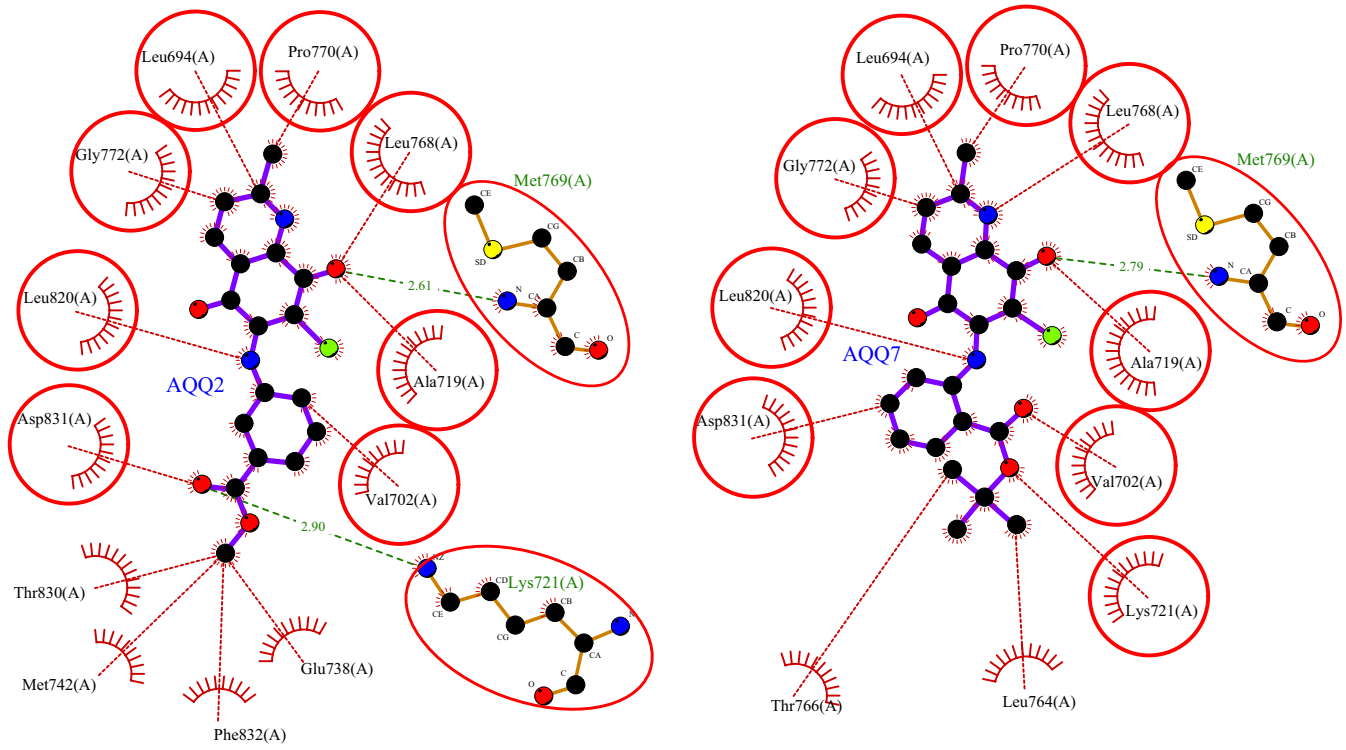

FIGURE 7 2D-interaction plot of **AQQ2** and **AQQ7** with epidermal growth factor receptor EGFR (PDB:1M17). The interacting residues common to both ligands are indicated by red circles. Arcs with red spikes indicate hydrophobic residues, dashed red lines indicate representative hydrophobic interactions, and dashed green lines indicate hydrogen-bonding interactions. The atoms of the amino acid residues and ligands are colored by atom type (carbon: black, oxygen: red, nitrogen: blue, sulfur: yellow, and chloro: green); the bonds of the amino acid residues are colored brown; and the ligands are colored violet.

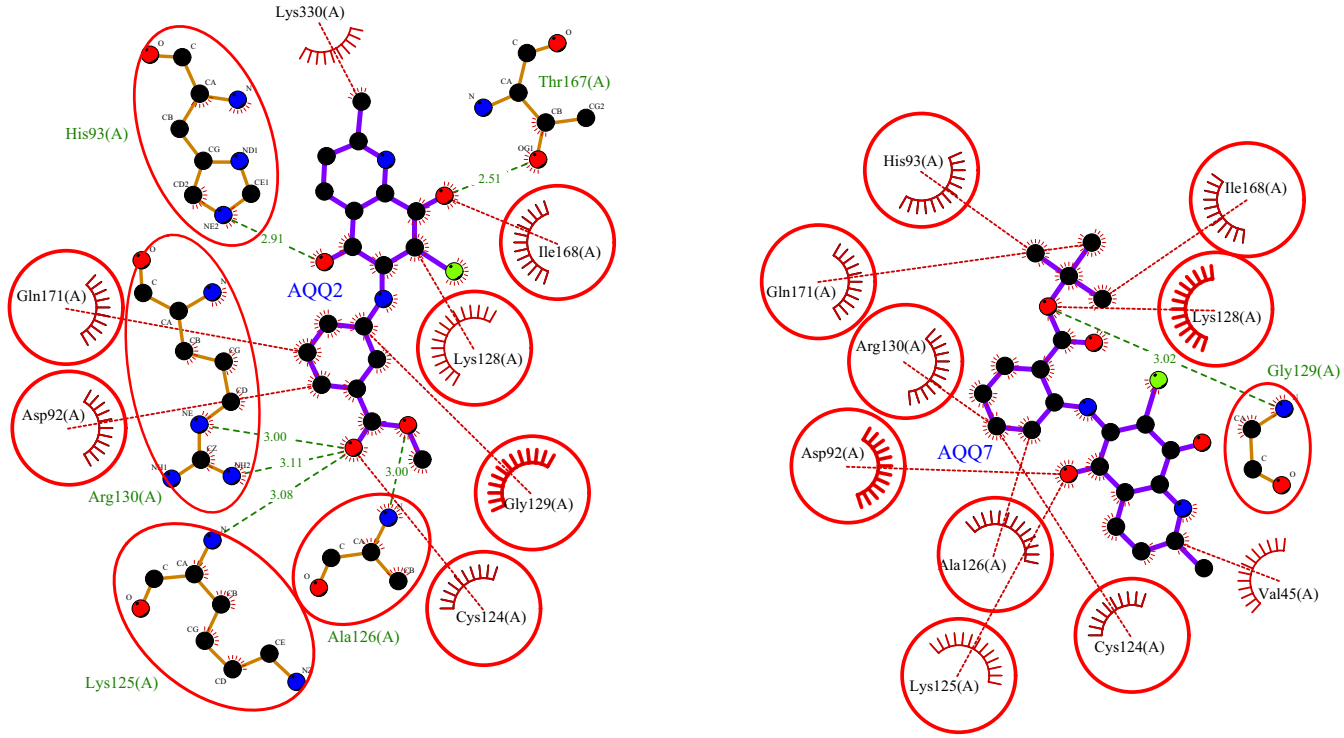

FIGURE 8 2D-interaction plot of **AQQ2** and **AQQ7** with Phosphatase and Tensin homolog (PTEN) (PDB:1D5R). The interacting residues common to both ligands are indicated by red circles. Arcs with red spikes indicate hydrophobic residues, dashed red lines indicate representative hydrophobic interactions, and dashed green lines indicate hydrogen-bonding interactions. The atoms of the amino acid residues and ligands are colored by atom type (carbon: black, oxygen: red, nitrogen: blue, sulfur: yellow, and chloro: green); the bonds of the amino acid residues are colored brown; and the ligands are colored violet.

ACKNOWLEDGMENTS

The authors are grateful to the National Cancer Institute (NCI), Bethesda, Maryland, USA, for carrying out the antiproliferative activity of the Developmental Therapeutics Program (DTP), Division of Cancer Treatment and Diagnosis, National Cancer Institute (http://dtp.cancer.gov).

CONFLICT OF INTEREST STATEMENT

The authors declare no conflicts of interest.

FUNDING INFORMATION

None.

DATA AVAILABILITY STATEMENT

The data that support the findings of this study are openly available in Developmental Therapeutics Program (DTP), Division of Cancer at http://dtp.cancer.gov.

REFERENCES

Adasme, M. F., Linnemann, K. L., Bolz, S. N., Kaiser, F., Salentin, S., Haupt, V. J., & Schroeder, M. (2021). PLIP 2021: Expanding the scope of the protein-ligand interaction profiler to DNA and RNA. *Nucleic Acids Research*, *49*(W1), W530–W534. https://doi.org/10.1093/nar/gkab294

Alfarouk, K. O., Stock, C. M., Taylor, S., Walsh, M., Muddathir, A. K., Verduzco, D., Bashir, A. H., Mohammed, O. Y., Elhassan, G. O., Harguindey, S., Reshkin, S. J., Ibrahim, M. E., & Rauch, C. (2015). Resistance to cancer chemotherapy: Failure in drug response from ADME to P-gp. *Cancer Cell International*, *15*, 71. https://doi.org/10.1186/s12935-015-0221-1

Ambrose, M., Ryan, A., Dunne, C., O'Sullivan, G. C., & Barry, O. P. (2005). Induction of apoptosis in 786-0 renal cell carcinoma by reactive oxygen species is ERK1/2-, p38δ and γ MAPK- and Pak-1-dependent but JNK-independent. *Cancer Research*, *65*(9_Supplement), 241.

Basset, G. J., Latimer, S., Fatihi, A., Soubeyrand, E., & Block, A. (2017). Phylloquinone (vitamin K1): Occurrence, biosynthesis and functions. *Mini Reviews in Medicinal Chemistry*, *17*(12), 1028–1038. https://doi.org/10.2174/1389557516666160623082714

Bayrak, N., Ciftci, H. I., Yildiz, M., Yildirim, H., Sever, B., Tateishi, H., Otsuka, M., Fujita, M., & Tuyun, A. F. (2021). Structure based design, synthesis, and evaluation of anti-CML activity of the quinolinequinones as LY83583 analogs. *Chemico-Biological Interactions*, *345*, 109555. https://doi.org/10.1016/j.cbi.2021.109555

Bayrak, N., Yildirim, H., Yildiz, M., Radwan, M. O., Otsuka, M., Fujita, M., Tuyun, A. F., & Ciftci, H. I. (2019). Design, synthesis, and biological activity of Plastoquinone analogs as a new class of anticancer agents. *Bioorganic Chemistry*, *92*, 103255. https://doi.org/10.1016/j.bioorg.2019.103255

Bayrak, N., Yildirim, H., Yildiz, M., Radwan, M. O., Otsuka, M., Fujita, M., Ciftci, H. I., & Tuyun, A. F. (2020). A novel series of

chlorinated plastoquinone analogs: Design, synthesis, and evaluation of anticancer activity. *Chemical Biology & Drug Design*, *95*(3), 343–354. https://doi.org/10.1111/cbdd.13651

Borba-Santos, L. P., Nicoletti, C. D., Vila, T., Ferreira, P. G., Araujo-Lima, C. F., Galvao, B. V. D., Felzenszwalb, I., de Souza, W., de Carvalho da Silva, F., Ferreira, V. F., Futuro, D. O., & Rozental, S. (2022). A novel naphthoquinone derivative shows selective antifungal activity against Sporothrix yeasts and biofilms. *Brazilian Journal of Microbiology*, *53*(2), 749–758. https://doi.org/10.1007/s42770-022-00725-1

Boyd, M. R., & Paull, K. D. (1995). Some practical considerations and applications of the national cancer institute in vitro anticancer drug discovery screen. *Drug Development Research*, *34*(2), 91–109. https://doi.org/10.1002/ddr.430340203

Brady, S. W., Gout, A. M., & Zhang, J. (2022). Therapeutic and prognostic insights from the analysis of cancer mutational signatures. *Trends in Genetics*, *38*(2), 194–208. https://doi.org/10.1016/j.tig.2021.08.007

Carneiro, B. A., & El-Deiry, W. S. (2020). Targeting apoptosis in cancer therapy. *Nature Reviews. Clinical Oncology*, *17*(7), 395–417. https://doi.org/10.1038/s41571-020-0341-y

Cheung-Ong, K., Giaever, G., & Nislow, C. (2013). DNA-damaging agents in cancer chemotherapy: Serendipity and chemical biology. *Chemistry & Biology*, *20*(5), 648–659. https://doi.org/10.1016/j.chembiol.2013.04.007

Ciftci, H., Sever, B., Bayrak, N., Yildiz, M., Yildirim, H., Tateishi, H., Otsuka, M., Fujita, M., & TuYuN, A. F. (2022). In vitro cytotoxicity evaluation of Plastoquinone analogues against colorectal and breast cancers along with In Silico insights. *Pharmaceuticals (Basel)*, *15*(10), 1266. https://doi.org/10.3390/ph15101266

Ciftci, H., Sever, B., Ocak, F., Bayrak, N., Yildiz, M., Yildirim, H., DeMirci, H., Tateishi, H., Otsuka, M., Fujita, M., & TuYuN, A. F. (2022). In vitro and in silico study of analogs of plant product Plastoquinone to be effective in colorectal cancer treatment. *Molecules*, *27*(3), 693. https://doi.org/10.3390/molecules27030693

Ciftci, H. I., Bayrak, N., Yildirim, H., Yildiz, M., Radwan, M. O., Otsuka, M., Fujita, M., & Tuyun, A. F. (2019). Discovery and structure-activity relationship of plastoquinone analogs as anticancer agents against chronic myelogenous leukemia cells. *Archiv der Pharmazie (Weinheim)*, *352*(12), e1900170. https://doi.org/10.1002/ardp.201900170

Cuartas, V., Aragon-Muriel, A., Liscano, Y., Polo-Ceron, D., Crespo-Ortiz, M. D. P., Quiroga, J., Abonia, R., & Insuasty, B. (2021). Anticancer activity of pyrimidodiazepines based on 2-chloro-4-anilinoquinazoline: Synthesis, DNA binding and molecular docking. *RSC Advances*, *11*(38), 23310–23329. https://doi.org/10.1039/d1ra03509f

Dahlem Junior, M. A., Nguema Edzang, R. W., Catto, A. L., & Raimundo, J. M. (2022). Quinones as an efficient molecular scaffold in the antibacterial/antifungal or Antitumoral arsenal. *International Journal of Molecular Sciences*, *23*(22), 14108. https://doi.org/10.3390/ijms232214108

Dasari, K., Somarelli, J. A., Kumar, S., & Townsend, J. P. (2021). The somatic molecular evolution of cancer: Mutation, selection, and epistasis. *Progress in Biophysics and Molecular Biology*, *165*, 56–65. https://doi.org/10.1016/j.pbiomolbio.2021.08.003

Di Marco, N. I., Paez, P. L., Lucero-Estrada, C. S. M., & Pungitore, C. R. (2021). Naphthoquinones inhibit formation and viability of Yersinia enterocolitica biofilm. *World Journal of Microbiology and Biotechnology*, *37*(2), 30. https://doi.org/10.1007/s11274-020-02971-7

Dos Santos, J. P. S., Ribeiro, R. C. B., Faria, J. V., Bello, M. L., Lima, C. G. S., Pauli, F. P., Borges, A. A., Rocha, D. R., Moraes, M. G., Forezi, L. S. M., Ferreira, V. F., Faria, R. X., & da Silva, F. C. (2022). Synthesis, biological evaluation and molecular modeling studies of novel 1,2,3-triazole-linked menadione-furan derivatives as P2X7 inhibitors. *Journal of Bioenergetics and Biomembranes*, *54*(5–6), 227–239. https://doi.org/10.1007/s10863-022-09947-2

Gonzalez-Conchas, G. A., Rodriguez-Romo, L., Hernandez-Barajas, D., Gonzalez-Guerrero, J. F., Rodriguez-Fernandez, I. A., Verdines-Perez, A., Templeton, A. J., Ocana, A., Seruga, B., Tannock, I. F., Amir, E., & Vera-Badillo, F. E. (2018). Epidermal growth factor receptor overexpression and outcomes in early breast cancer: A systematic review and a meta-analysis. *Cancer Treatment Reviews*, *62*, 1–8. https://doi.org/10.1016/j.ctrv.2017.10.008

Grever, M. R., Schepartz, S. A., & Chabner, B. A. (1992). The National Cancer Institute: Cancer drug discovery and development program. *Seminars in Oncology*, *19*(6), 622–638. Retrieved from https://www.ncbi.nlm.nih.gov/pubmed/1462164

Gupta, R., Luxami, V., & Paul, K. (2021). Insights of 8-hydroxyquinolines: A novel target in medicinal chemistry. *Bioorganic Chemistry*, *108*, 104633. https://doi.org/10.1016/j.bioorg.2021.104633

Harris, R. E., Casto, B. C., & Harris, Z. M. (2014). Cyclooxygenase-2 and the inflammogenesis of breast cancer. *World Journal of Clinical Oncology*, *5*(4), 677–692. https://doi.org/10.5306/wjco.v5.i4.677

Hirsch, F. R., Varella-Garcia, M., Bunn, P. A., Jr., Di Maria, M. V., Veve, R., Bremmes, R. M., Baron, A. E., Zeng, C., & Franklin, W. A. (2003). Epidermal growth factor receptor in non-small-cell lung carcinomas: Correlation between gene copy number and protein expression and impact on prognosis. *Journal of Clinical Oncology*, *21*(20), 3798–3807. https://doi.org/10.1200/JCO.2003.11.069

Holohan, C., Van Schaeybroeck, S., Longley, D. B., & Johnston, P. G. (2013). Cancer drug resistance: An evolving paradigm. *Nature Reviews. Cancer*, *13*(10), 714–726. https://doi.org/10.1038/nrc3599

Housman, G., Byler, S., Heerboth, S., Lapinska, K., Longacre, M., Snyder, N., & Sarkar, S. (2014). Drug resistance in cancer: An overview. *Cancers (Basel)*, *6*(3), 1769–1792. https://doi.org/10.3390/cancers6031769

Ibacache, J. A., Valderrama, J. A., Arancibia, V., Theoduloz, C., Muccioli, G. G., & Benites, J. (2016). Antiproliferative activity of new 6-bromine derivatives of 7-Anilino-1-Arylisoquinolineq uinones. *Journal of the Chilean Chemical Society*, *61*(4), 3191–3194. https://doi.org/10.4067/s0717-97072016000400008

Ibis, C., Tuyun, A. F., Ozsoy-Gunes, Z., Bahar, H., Stasevych, M. V., Musyanovych, R. Y., Komarovska-Porokhnyavets, O., & Novikov, V. (2011). Synthesis and biological evaluation of novel nitrogen- and sulfur-containing hetero-1,4-naphthoquinones as potent antifungal and antibacterial agents. *European Journal of Medicinal Chemistry*, *46*(12), 5861–5867. https://doi.org/10.1016/j.ejmech.2011.09.048

Jannuzzi, A. T., Yildiz, M., Bayrak, N., Yildirim, H., Shilkar, D., Jayaprakash, V., & TuYuN, A. F. (2021). Anticancer agents based on Plastoquinone analogs with N-phenylpiperazine:

Structure-activity relationship and mechanism of action in breast cancer cells. *Chemico-Biological Interactions*, *349*, 109673. https://doi.org/10.1016/j.cbi.2021.109673

Jannuzzi, A. T., Yilmaz Goler, A. M., Bayrak, N., Yildiz, M., Yildirim, H., Karademir Yilmaz, B., Shilkar, D., Venkatesan, R. J., Jayaprakash, V., & TuYuN, A. F. (2022). Exploring the anticancer effects of brominated plastoquinone analogs with promising cytotoxic activity in MCF-7 breast cancer cells via cell cycle arrest and oxidative stress induction. *Pharmaceuticals (Basel)*, *15*(7), 777. https://doi.org/10.3390/ph15070777

Kadela, M., Jastrzebska, M., Bebenek, E., Chrobak, E., Latocha, M., Kusz, J., Ksiazek, M., & Boryczka, S. (2016). Synthesis, structure and cytotoxic activity of mono- and Dialkoxy derivatives of 5,8-Quinolinedione. *Molecules*, *21*(2), 156. https://doi.org/10.3390/molecules21020156

Kara, E. M., Bayrak, N., Yildirim, H., Yildiz, M., Celik, B. O., & Tuyun, A. F. (2020). Chlorinated plastoquinone analogs that inhibit Staphylococcus epidermidis and Candida albicans growth. *Folia Microbiologia (Praha)*, *65*(5), 785–795. https://doi.org/10.1007/s12223-020-00783-8

Kim, S. J., Kim, H. S., & Seo, Y. R. (2019). Understanding of ROS-inducing strategy in anticancer therapy. *Oxidative Medicine and Cellular Longevity*, *2019*, 5381692. https://doi.org/10.1155/2019/5381692

Kim, Y. S., Park, S. Y., Lee, H. J., Suh, M. E., Schollmeyer, D., & Lee, C. O. (2003). Synthesis and cytotoxicity of 6,11-dihydro-pyrido- and 6,11-dihydro-benzo[2,3-b]phenazine-6,11-dione derivatives. *Bioorganic & Medicinal Chemistry*, *11*(8), 1709–1714. https://doi.org/10.1016/s0968-0896(03)00028-2

Kimura, Y. (2005). New anticancer agents: In vitro and in vivo evaluation of the antitumor and antimetastatic actions of various compounds isolated from medicinal plants. *In Vivo*, *19*(1), 37–60. Retrieved from <Go to ISI>://WOS:000227883600004.

Laskowski, R. A., & Swindells, M. B. (2011). *LigPlot+: Multiple ligand–protein interaction diagrams for drug discovery*. ACS Publications.

Lima, C. G. S., de Souza, A. S., Pauli, F. P., Ribeiro, R. C. B., Borges, A. d. A., Ferreira, P. G., da Silva, F. d. C., Ferreira, V. F., & da Forezi, L. S. M. (2021). Functional group transformation in naphthoquinones: Strategies for the synthesis of mono- and Bis(Amino-1,4-naphthoquinones). *Current Organic Chemistry*, *25*(19), 2156–2174. https://doi.org/10.2174/1385272825666210811121450

Lopez-Lira, C., Tapia, R. A., Herrera, A., Lapier, M., Maya, J. D., Soto-Delgado, J., Oliver, A. G., Graham Lappin, A., & Uriarte, E. (2021). New benzimidazolequinones as trypanosomicidal agents. *Bioorganic Chemistry*, *111*, 104823. https://doi.org/10.1016/j.bioorg.2021.104823

Mahalapbutr, P., Leechaisit, R., Thongnum, A., Todsaporn, D., Prachayasittikul, V., Rungrotmongkol, T., Prachayasittikul, S., Ruchirawat, S., Prachayasittikul, V., & Pingaew, R. (2022). Discovery of Anilino-1,4-naphthoquinones as potent EGFR tyrosine kinase inhibitors: Synthesis, biological evaluation, and comprehensive molecular modeling. *ACS Omega*, *7*(21), 17881–17893. https://doi.org/10.1021/acsomega.2c01188

Majolo, F., de Oliveira Becker Delwing, L. K., Marmitt, D. J., Bustamante-Filho, I. C., & Goettert, M. I. (2019). Medicinal plants and bioactive natural compounds for cancer treatment: Important advances for drug discovery. *Phytochemistry Letters*, *31*, 196–207. https://doi.org/10.1016/j.phytol.2019.04.003

Markopoulos, G. S., Roupakia, E., Tokamani, M., Chavdoula, E., Hatziapostolou, M., Polytarchou, C., Marcu, K. B., Papavassiliou, A. G., Sandaltzopoulos, R., & Kolettas, E. (2017). A step-by-step microRNA guide to cancer development and metastasis. *Cellular Oncology (Dordrecht)*, *40*(4), 303–339. https://doi.org/10.1007/s13402-017-0341-9

Mctigue, M. A., Davies, J. F., II, Kaufman, B. T., Xuong, N.-H., & Kraut, J. (1993). Crystal structures of Organomercurial-activated chicken liver Dihydrofolate reductase complexes. Publication no. https://doi.org/10.2210/pdb1DR5/pdb)

Monks, A., Scudiero, D., Skehan, P., Shoemaker, R., Paull, K., Vistica, D., Hose, C., Langley, J., Cronise, P., Vaigro-Wolff, A., Gray-Goodrich, M., Campbell, H., Mayo, J., & Boyd, M. (1991). Feasibility of a high-flux anticancer drug screen using a diverse panel of cultured human tumor cell lines. *Journal of the National Cancer Institute*, *83*(11), 757–766. https://doi.org/10.1093/jnci/83.11.757

Nagar, B., & Dhar, B. B. (2022). Visible light-mediated Thiolation of substituted 1,4-naphthoquinones using eosin Y as a Photoredox catalyst. *The Journal of Organic Chemistry*, *87*(5), 3195–3201. https://doi.org/10.1021/acs.joc.1c02924

Okeke, I. N., Klugman, K. P., Bhutta, Z. A., Duse, A. G., Jenkins, P., O'Brien, T. F., Pablos-Mendez, A., & Laxminarayan, R. (2005). Antimicrobial resistance in developing countries. Part II: Strategies for containment. *The Lancet Infectious Diseases*, *5*(9), 568–580. https://doi.org/10.1016/S1473-3099(05)70217-6

Pauli, F. P., Freitas, C. S., Pereira, P. R., Magalhaes, A., de Carvalho da Silva, F., Paschoalin, V. M. F., & Ferreira, V. F. (2023). Exploring the antimicrobial and Antitumoral activities of naphthoquinone-grafted Chitosans. *Polymers (Basel)*, *15*(6), 1430. https://doi.org/10.3390/polym15061430

Pettersen, E., Goddard, T., Huang, C., Couch, G., Greenblatt, D., Meng, E., & Ferrin, T. (2004). UCSF chimera–A visualization system for exploratory research and analysis. *Journal of Computational Chemistry*, *25*(13), 1605–1612.

Razaghi, A., Heimann, K., Schaeffer, P. M., & Gibson, S. B. (2018). Negative regulators of cell death pathways in cancer: Perspective on biomarkers and targeted therapies. *Apoptosis*, *23*(2), 93–112. https://doi.org/10.1007/s10495-018-1440-4

Ricci, M. S., & Zong, W. X. (2006). Chemotherapeutic approaches for targeting cell death pathways. *The Oncologist*, *11*(4), 342–357. https://doi.org/10.1634/theoncologist.11-4-342

Shaikh, I. A., Johnson, F., & Grollman, A. P. (1986). Streptonigrin. 1. Structure-activity relationships among simple bicyclic analogues. Rate dependence of DNA degradation on quinone reduction potential. *Journal of Medicinal Chemistry*, *29*(8), 1329–1340. https://doi.org/10.1021/jm00158a002

Song, G., Zhong, B., Zhang, B., Rehman, A. U., & Chen, H. F. (2023). Phosphorylation modification force field FB18CMAP improving conformation sampling of phosphoproteins. *Journal of Chemical Information and Modeling*, *63*(5), 1602–1614. https://doi.org/10.1021/acs.jcim.3c00112

Stamos, J., Sliwkowski, M. X., & Eigenbrot, C. (2002). Structure of the epidermal growth factor receptor kinase domain alone and in complex with a 4-anilinoquinazoline inhibitor. *The Journal of Biological Chemistry*, *277*(48), 46265–46272. https://doi.org/10.1074/jbc.M207135200

Uysal, S., Soyer, Z., Saylam, M., Tarikogullari, A. H., Yilmaz, S., & Kirmizibayrak, P. B. (2021). Design, synthesis and biological evaluation of novel naphthoquinone-4-aminobenzensulfonamide/carboxamide derivatives as proteasome inhibitors. *European Journal of Medicinal Chemistry*, *209*, 112890. https://doi.org/10.1016/j.ejmech.2020.112890

Valdes-Tresanco, M. S., Valdes-Tresanco, M. E., Valiente, P. A., & Moreno, E. (2020). AMDock: A versatile graphical tool for assisting molecular docking with Autodock Vina and Autodock4. *Biology Direct*, *15*(1), 12. https://doi.org/10.1186/s13062-020-00267-2

van Oijen, M. G., & Slootweg, P. J. (2000). Gain-of-function mutations in the tumor suppressor gene p53. *Clinical Cancer Research*, *6*(6), 2138–2145.

Varricchio, C., Beirne, K., Aeschlimann, P., Heard, C., Rozanowska, M., Votruba, M., & Brancale, A. (2020). Discovery of novel 2-Aniline-1,4-naphthoquinones as potential new drug treatment for Leber's hereditary optic neuropathy (LHON). *Journal of Medicinal Chemistry*, *63*(22), 13638–13655. https://doi.org/10.1021/acs.jmedchem.0c00942

Veronesi, U., & Boyle, P. (2017). Breast cancer. In S. R. Quah (Ed.), *International encyclopedia of public health* (pp. 272–280). Academic Press.

Wellington, K. W. (2015). Understanding cancer and the anticancer activities of naphthoquinones – A review. *RSC Advances*, *5*(26), 20309–20338. https://doi.org/10.1039/c4ra13547d

World Cancer Day. (2021). Breast cancer overtakes lung cancer in terms of number of new cancer cases worldwide. Retrieved from https://www.iarc.who.int/infographics/world-cancer-day-2021/

Xu, S., Uddin, M. J., Banerjee, S., Duggan, K., Musee, J., Kiefer, J. R., Ghebreselasie, K., Rouzer, C. A., & Marnett, L. J. (2019). Fluorescent indomethacin-dansyl conjugates utilize the membrane-binding domain of cyclooxygenase-2 to block the opening to the active site. *The Journal of Biological Chemistry*, *294*(22), 8690–8698. https://doi.org/10.1074/jbc.RA119.007405

Yildirim, H., Bayrak, N., Yildiz, M., Mataraci-Kara, E., Korkmaz, S., Shilkar, D., Jayaprakash, V., & TuYuN, A. F. (2022). Aminated Quinolinequinones as privileged scaffolds for antibacterial agents: Synthesis, In vitro evaluation, and putative mode of action. *ACS Omega*, *7*(46), 41915–41928. https://doi.org/10.1021/acsomega.2c03193

Yilmaz Goler, A. M., Jannuzzi, A. T., Bayrak, N., Yildiz, M., Yildirim, H., Otsuka, M., Fujita, M., Radwan, M. O., & TuYuN, A. F. (2022). In vitro and In Silico study to assess toxic mechanisms of hybrid molecules of Quinone-benzocaine as Plastoquinone analogues in breast cancer cells. *ACS Omega*, *7*(34), 30250–30264. https://doi.org/10.1021/acsomega.2c03428

SUPPORTING INFORMATION

Additional supporting information can be found online in the Supporting Information section at the end of this article.

How to cite this article: Jannuzzi, A. T., Yilmaz Goler, A. M., Shilkar, D., Mondal, S., Basavanakatti, V. N., Yıldırım, H., Yıldız, M., Çelik Onar, H., Bayrak, N., Jayaprakash, V., & TuYuN, A. F. (2023). Cytotoxic activity of quinolinequinones in cancer: In vitro studies, molecular docking, and ADME/PK profiling. *Chemical Biology & Drug Design*, *00*, 1–22. https://doi.org/10.1111/cbdd.14314